Single Azobenzene Main Chain Polymers on Nanostructured Molecular Monolayers: Immobilization, Alignment and Light-Induced Movements

Dissertation

zur Erlangung des akademischen Grades
doctor rerum naturalium
(Dr. rer. nat.)
im Fach Physik

Spezialisierung: Experimentalphysik

eingereicht an der
Mathematisch-Naturwissenschaftlichen Fakultät
der Humboldt-Universität zu Berlin

von

Chien-Li Lee, M. Sc.

Präsidentin der Humboldt-Universität zu Berlin
Prof. Dr.-Ing. Dr. Sabine Kunst

Dekan der Mathematisch-Naturwissenschaftlichen Fakultät
Prof. Dr. Elmar Kulke

(Erst nach der Disputation für die Veröffentlichung in der Universitaätsbibliothek gemäß § 15 die Namen und das Datum eintragen):

Gutachter/innen:
1. Prof. Dr. Jürgen P. Rabe
2. Prof. Dr. Stefan Kowarik
3. Prof. Dr. Svetlana Santer

Tag der mündlichen Prüfung: 28.06.2017

Abstract

For generations, scientists have been inspired by sophisticated molecular systems, which can harness solar energy for various physiological processes. By means of synthetic molecular photoswitches, we now have the potential to catch up with nature in many ways, with the ultimate goal of constructing light-controlled, so called molecular machines that are capable of performing tasks at the molecular scale. An important challenge in developing such artificial molecular machines is attaining a detailed understanding and possibly control of photoisomerization-coupled molecular movements within macromolecular architectures, whiling taking the influence of the local environments into account. In this thesis, I use scanning force microscopy (SFM) to provide insights into the behavior of individual photoresponsive macromolecules physisorbed on a surface and to identify light-induced movements such as contraction, extension, and crawling events. Thereby, the specific local environments provided by the molecular surface not only serve to isolate and orient the macromolecules but also function as a template that influences the directions of molecular movements.

This work presents a comprehensive investigation of one particular photoresponsive macromolecule: Azobenzene photoswitches incorporated into the backbone of synthetic rigid-rod polymers. Firstly, the polymers were deposited from solution onto a monolayer of octadecylamine (ODA) covering the basal plane of highly oriented pyrolytic graphite (HOPG). The unique ODA amphiphilic nanorails, self-assembled on HOPG, served not only to immobilize and isolate the polymers, but also to orient them on the surface. The orientations of rod-like polymers on an ODA surface, i.e., predominally perpendicular or parallel with respect to the underlying lamellar surface, were analyzed with a model based on the hydrophobic interaction of the side chains of the polymers with the amphiphilic nanorails of the ODA molecules. Upon the irradiations with UV and visible light, respectively, large light-induced contractions and extensions of the single macromolecules have been visualized by SFM. Upon contraction, the average polymer chain lengths shrunk by 60% and formed more compact nanostructures. An SFM's time-laps study of morphological changes of polymers at different irradiating times also detailed the light-induced movements within the macromolecules and a crawling movement across the surface. Those light-induced motions were attributed to a weak mechanical and electronic coupling between the surface and the polymers, the high density of azobenzenes in their backbones, and their rigidity, allowing for maximized photodeformations. Moreover, the influence of local environments on light-induced molecular movements was further investigated by repetitively switching the single polymers on different sites of a heterogeneous ODA surface. For weakly adsorbed polymers on surface defects, those surface-directed folding/unfolding (or contracting/extending) movements exhibited a random change in orientation. Thus, I conclude, that well-defined local environments, such as domain boundaries or lamellae within the ODA monolayer, play important roles in the template that directs the folding and unfolding movements of polymers during irradiation. The developed setup allows to promote the development of optomechanical nanosystems by optimizing the interaction between single macromolecules and ODA surfaces, followed by visualization of light-induced, on-surface motions of single macromolecules.

Zusammenfassung

Hochentwickelte molekulare Systeme, die Sonnenlicht für unterschiedlichste physiologische Prozesse nutzbar machen können, haben die Wissenschaft seit Generationen beeindruckt. Mit Hilfe synthetischer molekularer Photoschalter besteht nun die Möglichkeit, mit der Natur in vielen Bereichen nachzuziehen. Das große Ziel dabei ist die Entwicklung von mit Licht angetriebenen molekularen Maschinen, die auf molekularer Ebene Aufgaben erfüllen können. Eine große Herausforderung ist das Verständnis und möglicherweise auch die Kontrolle der Bewegung makromolekularer Systeme während ihrer Photoisomerisierung unter Berücksichtigung von Umgebungseinflüssen. In der vorliegenden Arbeit habe ich das Verhalten von einzelnen licht-empfindlichen Makromolekülen auf Oberflächen mit Hilfe von Rasterkraftmikroskopie (SFM) untersucht und lichtinduzierte Bewegungen wie Kontraktion, Expansion und Kriechbewegungen identifiziert. Dabei diente die spezielle Umgebung einer molekularen physisorbierten Monoschicht auf einer glatten Festkörperoberfläche eine wichtige Rolle sowohl zur Vereinzelung und Ausrichtung der Makromoleküle, wie auch zur Beeinflussung von deren Bewegungsrichtung.

Die vorliegende Arbeit präsentiert eine umfassende Untersuchung zu einem speziellen lichtempfindlichen Makromolekül: ein Azobenzol Photoschalter, eingebettet in den Hauptstrang eines synthetischen stäbchenförmigen Polymers. Dazu wurden die Polymere zunächst aus Lösung auf eine Einfachlage Octadecylamin (ODA) aufgebracht, welche auf einer Oberfläche von hochgeordnetem pyrolytischem Graphit (HOPG) lag. Die besondere Eigenschaft der amphiphilen ODAs, sich in Nanolamellen anzuordnen, diente nicht nur der Immobilisierung und Isolierung der stabförmigen Polymere, sondern auch deren Orientierung auf der Oberfläche. Diese Orientierung, insbesondere die Ausrichtung relativ zu den Lamellen, wurde mit einem Modell, basierend auf den hydrophoben Wechselwirkungen zwischen den Seitenketten der Polymere und der amphiphilen Unterlage aus ODA, untersucht. Mittels SFM konnte die Kontraktion beziehungsweise Expansion bei Belichtung mit UV- oder sichtbarem Licht untersucht werden. Bei Kontraktion schrumpfte die Länge der Polymere im Mittel um 60% und es bildeten sich kompaktere Nanostrukturen. In zeitaufgelösten Messungen wurden lichtinduzierte morphologische Änderungen in Abhängigkeit von der Belichtungszeit der Polymere gemessen. Dies verdeutlichte die lichtinduzierte Bewegung dieser Strukturen innerhalb der Makromoleküle und offenbarte eine kriechende Fortbewegung der Polymere über die Oberfläche. Dies wurde auf eine schwache mechanische und elektrische Kopplung zwischen Oberfläche und Makromolekül zurückgeführt. Zusätzlich führt die hohe Dichte an Azobenzolgruppen im Rückgrat der Makromoleküle und deren Steifheit zu einer erhöhten lichtinduzierten Verformung. Außerdem wurde der Einfluss der lokalen Umgebung auf diese Bewegungen durch mehrmaliges Hin- und Herschalten der Polymere auf unterschiedlichen Stellen einer heterogenen ODA Oberfläche untersucht. Polymere, die auf Oberflächendefekten nur schwach gebunden waren, änderten ihre Orientierung bei Belichtung zufällig. Daraus schlussfolgere ich, dass die wohldefinierte lokale Umgebung mit Korngrenzen oder Lamellen eine wichtige Rolle als Templat spielt und die Bewegungsrichtung maßgeblich bestimmt. Die entwickelte experimentelle Methode kann verwendet werden, um die Wechselwirkungen zwischen Oberfläche und Polymer zu optimieren, und die anschließende Untersuchung von lichtinduzierten Bewegung der Makromoleküle kann die Entwicklung neuartiger optomechanischer Nanosysteme ermöglichen.

Table of Contents

Chapter 1

Introduction

1.1 Synthetic molecular machines

To sustain life and biological events, nature has developed molecular machines to drive virtually every biological process.[1] The ubiquitous presence of naturally occurring molecular machines in living systems inspires and at the same time challenges scientists to design and construct synthetic motors and machines at the nanometer sale, that is, at the molecular level. The further development of molecular machines is predicted not only to promote the miniaturization in information storage, but also to open the new fields of smart drugs, smart materials and energy.

A synthetic molecular machine can be composed of a discrete number of molecular components to perform molecular movements under control of appropriate energy inputs.[1] Though construction of more complex molecular machines remains in the area of theoretical research, some outstanding synthetic molecular machines mimicking their macroscopic counterparts that perform mechanical movements, have been designed and realized such as, molecular motors,[2,3,4] molecular propellers,[5] molecular shuttles,[6,7,8] molecular tweezers[9,10] and nano-cars.[11–14]

Significant attention in studying synthetic molecular machines have been devoted to developing molecules that can undergo contracting/extending conformational changes in a manner reminiscent of human muscles.[7,15,16] Such muscle-like molecules that can transduce external stimuli into mechanical force have emerged as key

building blocks in constructing controllable nano- and mesoscale mechanical systems.[8,17] Utilizing these molecular-scale forces to perform useful tasks is of course the next challenging step.[3] Progress in this direction has been made, e.g., in optomechanical control of electron transfer in a azobenzene-linked diporphyrin Zn complex,[18] favoring different hydrogen-bonding networks,[19] cargo-lifting[20] and twisting of other smaller molecules.[10]

Inspired by muscular tissues where the microscopic contractions of thousands of myosin filaments gliding along thin acting filaments are able to produce large integrated contractions of the sacromeres, the translational motions of synthetic molecules that starts at the nanometer-scale could be likewise amplified with integrated motion by clever molecular designs, such as incorporating muscle-like molecules into the core of dendrimers[21–24] or polymerizing them into linear strands.[25,26] Depending on the degree of polymerization and effectiveness of the cumulative motion of individual molecules, the molecular movement can increase by orders of magnitude.[16,26] To this end, not only the molecules that perform contraction/extension are of interest, but also, equally important, the easiness of incorporating them into various molecular architectures to amplify the amplitude of their mechanical motions. In the past decades, some most versatile and extensively studied small-molecule motifs include (but are far from limited to) rotaxane and azobenzene which can adopt contracted/extended conformational change and at the same time, are ready to be incorporated into different molecular architectures or polymerized into linear strands. In the following section examples of current developments of rotaxane- and azobenzene-based molecular machines are presented able to perform large amplitude translational motions.

1.2 Single molecular machines performing large amplitude translational motions

Pioneering work in the development of linear molecular muscles has been on rotaxane-based molecular switches and shuttles.[27,28] [3]Rotaxanes[15] have been compared to linear molecular muscles (Figure 1.1a.b) because of the ability of their rings to slide between two or more recognition sites along their linear dumbbell portions in response to external stimuli, such as a chemical or electrochemical stimulus. Depending on the redox state, the rings find themselves either in contracted state (1.4 nm apart) or in extended state (4.2 nm apart). By anchoring these "molecular muscles" to a micro-sized gold beam[8] (Figure 1.1c), the bending of the cantilever beam up to tens of nanometers suggests that the cumulative effect of individual microscopic motions within [3]rotaxane molecules can be harnessed to perform larger-scale mechanical work. With the aim of integrating the contractions and extensions of individual molecules, Du *et. al.* polymerized thousands of tailored rotaxanes linearly to successfully integrate motion from thousands of molecular machines.[16] However, due to the small persistence length, the integrated contracting motions of the rotaxanes are translated to shrinkage of the coiled polymer in size rather than one-dimensional translational motion. Also the use of metal ions could cause difficulties in their further incorporation into other molecular components or interfacing them with other objects. The next challenges to access macroscopic responses in rotaxane-based molecules includes varying the persistence length of the polymers, and in bundling and orienting them in stiffer fibers, just as myofibrils do in muscles.

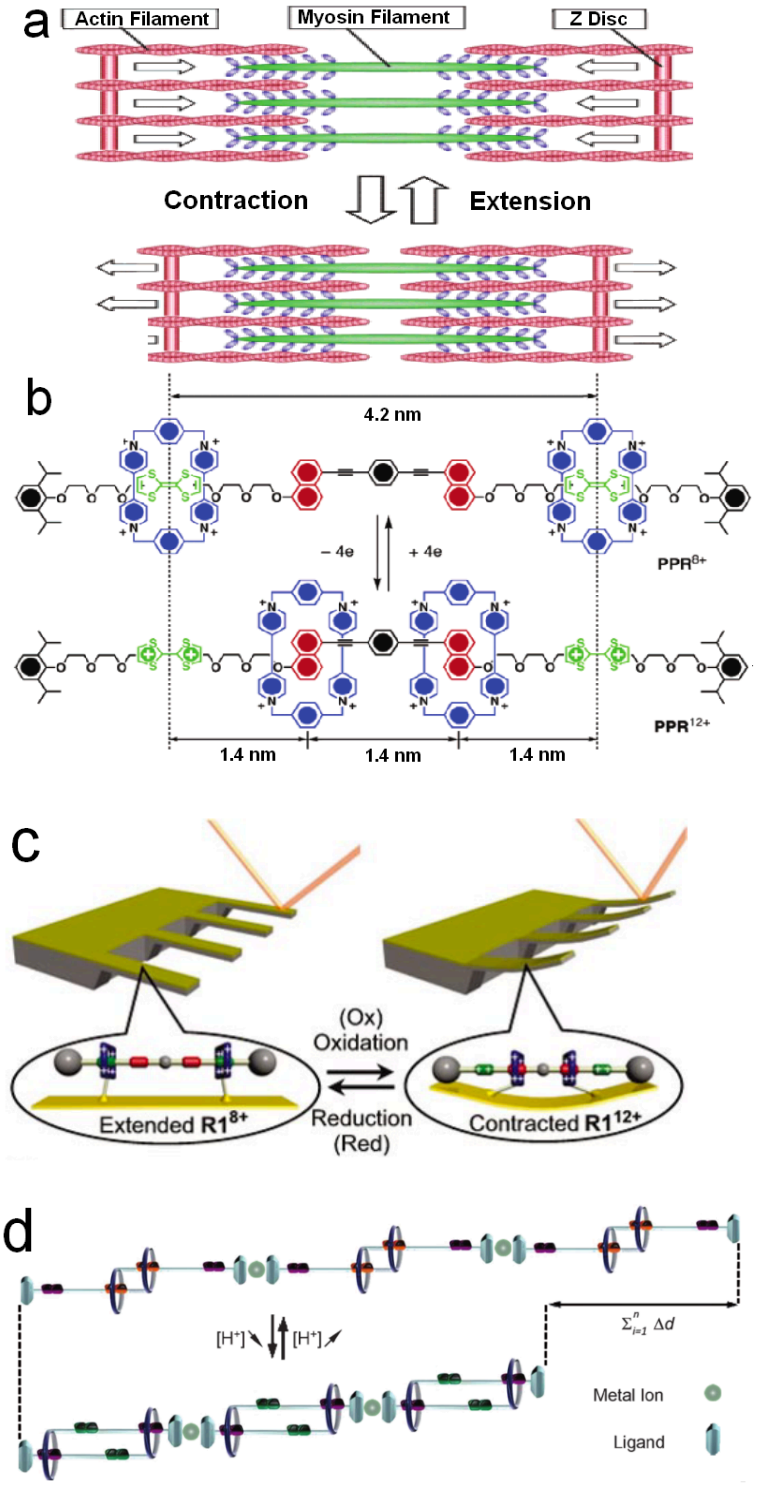

Figure 1.1 (a) Graphical representations of the constitution and cycle of contraction and extension of the sarcomeres in skeletal muscle. Schematic taken from Ref.[15] (b) Structural formulas of the contracted (**PPR^{8+}**) and the extended (**PPR^{12+}**) states of the prototypical molecular muscle. Schematic taken from Ref.[15] (c) Microcantilever beams, coated with a monolayer of [3]rotaxanes, undergo bending when they are exposed to chemical stimulus. Schematic taken from Ref.[8] (d) The integrated translational motion of the supramolecular polymer chain is the product of the individual contractions and extensions of [c2]daisy chain rotaxane by the degree of polymerization. Schematic taken from Ref.[16].

Similar to the rotaxane molecule, azobenzene is another, probably the most well-known muscle-like molecule that can perform translational motion. Through reversible conformational change between the extended *trans* and the contracted *cis* isomers, the distance between the substituents of azobenzene at the two ends reduces from 0.99 nm in the *trans* state to 0.55 nm in the *cis* state, a distance which is very large by molecular standards and therefore azobenzene holds potentials for constructing useful molecular machines. The ability of using light as a powerful external stimulus to control or trigger the translational motion makes azobenzene an attractive candidate for developing optomechanical molecular machines.

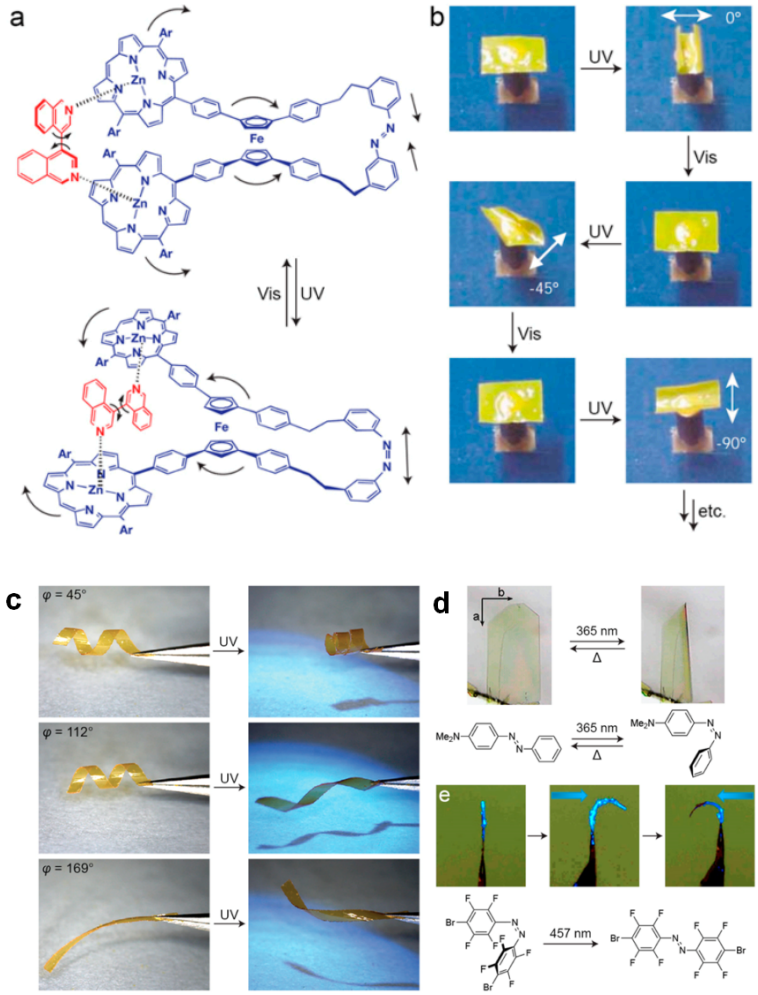

Figure 1.2 Selected examples of systems containing azobenzene that can perform large-amplitude motions by photoisomerization. (a) Light-operated molecular machine (blue) capable of mechanically twisting a small-molecule guest (red). Schematic reproduced from the Ref.[10] (b) Light-controlled bending of photoresponsive polymer film. White arrows indicate angles of polarization of linearly polarized UV light. Images reproduced from the Ref.[27] (c) Photoresponsive springs powered by nonpolarized UV light. Images taken from the Ref.[28] (d) Photoinduced folding of 4-(dimethylamino)azobenzene crystals. Reproduced from the Ref.[31] (e) Perhalogenated azobenzene crystal and its light-induced bending. Blue arrows indicate the direction of irradiation. Reproduced from the Ref.[32]

Some outstanding examples of optomechanical systems using azobenzene demonstrated that translational motion of azobenzene could be amplified and harnessed with clever molecular designs. For example, azobenzene has been smartly

incorporated into a "molecular scissor" that is able to perform large-amplitude motions and twist a guest of a smaller molecule (Figure 1.2a).[29,10] Similarly, azobenzene derivatives have been incorporated within a polymer film that can exhibit light-induced shape changes (Figure 1.2b)[30,31] and even perform rolling motions.[32] At the same time, significant attention has been devoted to amplifying individual molecular responses in highly oriented materials, such as single crystals: as the examples in Figure 1.2c,d show,[33,34,35] certain azobenzene crystals bend in response to light. Finally, azobenzene has been introduced into biological systems where various biomolecules functionalized with an azobenzene moiety can exhibit large conformational changes when exposed to light.[36,37]

Even though the macromolecular architectures incorporating multiple rotaxane or azobenzene molecules have shown the ability to perform large molecular movements, increasing the efficiency and controlling those movements in a precise way, require still a long way to go. In the following sections of this thesis, I will focus on a promising muscle-like polymer incorporating multiple azobenzenes in the main chain.

1.3 Challenges and motivation

One key challenge in developing molecular machines is to understand the detailed actuating movements within macromolecular architectures and the consequences of those movements with respect to the local environment, which requires the ability to isolate macromolecules in a well-defined environment and probe them individually. For this purpose, I intended to isolate a specific azo-polymer on a well-defined surface and to investigate its moving process in response to an external stimulus and the consequences of those movements with respect to the local environment. More specifically, I intended to tackle the following challenges:

First, there was still no "direct visualization" of single azobenzene-containing macromolecules (azobenzene-macromolecules) moving in response to light. Many studies on azobenzene-molecular systems are performed in bulk materials or in solutions, while studies on azobenzene-containing molecules (azobenzene-molecules) on surfaces are often in a monolayer[38] or embedded in another molecular matrix.[39,40] The observed movements are either from molecular ensembles or they are indirect induced by other molecules. In the real sense of imaging movements of azobenzene-molecules induced by stimuli, to our knowledge, only small individual azobenzene-molecules undergoing conformational change have been previously "visualized" on a clear single molecular level by surface probe microscopies.[41,42,43,4445,46] Here I intended to "visualize" well-isolated azobenzene-macromolecules undergoing conformational changes by scanning force microscopy. The visualization of single molecules could increase their addressability and processability, as required of molecular machines. It should be noted that another example of this kind, reported by Baigl and coworkers,[47] details the *indirect* light-fueled compaction of DNA.

Second, the efficiency of transducing photons into large mechanical movements of azobenzene-macromolecules could be improved. Due to incomplete isomerization of the polymer, the previous study on bending an SFM beam falls short of its theoretical maximum in terms of bending deflection.[17] This suggests an increased conversion efficiency of the azobenzene-polymer is needed for future mechano-optical devices. Recently, much attention has been devoted to maximizing the photodeformation of individual molecules by more efficient isomerization and high-density configurations.[48] The experiments of these azobenzene polymers in solutions showed an unprecedented decrease in hydrodynamic volume as a result of

photoisomerization. Here in this thesis, I tried to measure the actual contraction/extension within these single isolated polymers and to demonstrate that larger translational movement within single macromolecules can be achieved.

Third, despite of smart incorporations of azobenzenes in various macromolecular architectures and their applications that are emerging, the consequences of the isomerization within azobenzene-macromolecules and with the surroundings could be better understood. Although azobenzene switching on a single molecule level has been observed before using scanning probe microscopies, all these experiments were performed on thiolated azobenzenes fixed covalently onto metallic surfaces, consequently, no movements other than switching of azobenzene were observed. By isomerizing unbound molecules deposited *noncovalently* on a surface, it is possible to observe some very interesting consequences of the isomerization process, such as a folding/contraction process, on-surface movements as well as extension as result of back-isomerization.

Finally, it is very challenging to switch azobenzene on a surface. For example, the lack of freedom for conformational change and strong coupling both mechanically and electronically with the underlying surface can all significantly impair the photoisomerization process.

In this thesis I will address the above-mentioned challenges by focusing on one particular synthetic rigid-rod polymers incorporating multiple azobenzene photoswitches in the backbone (see **P1**, Figure 3.1) deposited from solution onto a monolayer of octadecylamine covering the basal plane of graphite. For this interesting polymer the following will be shown:

(1) Single **P1** polymers could be immobilized, isolated and orientated on a well-defined ODA monolayer.

(2) A model based on the hydrophobic interaction of side chains of polymers with an amphiphilic surface has been suggested to explain the alignments of the polymers on the surface.

(3) Direct visualization of large translational motion within single macromolecules resulting from the folding/contraction process and the extension as a result of back-isomerization.

(4) Demonstration of crawling movement as a consequence of phtoisomerization.

(5) Demonstration of surface-directed folding/unfolding of a single polymer and the repetitive contraction/extension of single polymers on different sites of a heterogeneous amphiphilic surface.

The structure of this thesis is the following. Chapter 2 introduces basic azobenzene photochemistry, the molecular motion of azobenzene, the determination of the mechanical force performed by a single azobenzene-polymer, maximizing the photodeformation of individual molecules and the fundamental mechanism of formation of octadecylamine (ODA) self-assembled monolayer on a graphite surface. Chapter 3.1 introduces the details of the material we use, namely, the azobenzene main chain polymer (**P1**) and it reviews polymers' characterization in solution, such as UV-Vis absorption spectroscopy, NMR titration for determination of the PSS (Photo Stationary State), aggregation and disruption of **P1** polymers in solutions, as reported previously. Chapter 3.2 covers sample preparation and experimental setups of scanning force microscopy (SFM) and light sources. The results and discussion provided in Chapter 4 are divided into three subjects. Chapter 4.1 demonstrates the different alignments of isolated single polymers on ODA surfaces and proposes a

model based on hydrophobic interaction to explain it. Chapter 4.2 demonstrates the results of light-induced contraction and extension of single macromolecules on a surface as well as an interesting crawling movement. Chapter 4.3 demonstrates the repetitive switching of macromolecules on the surface and discusses the role of the heterogeneous ODA surface in directing the movements of polymer. Chapter 5 provides the summary and outlook.

Chapter 2

Fundamentals

2.1 Photoswitchable azobenzene-containing polymers

2.1.1 Azobenzene photochemistry

Azobenzene is an aromatic molecule formed by an azo bond (–N=N–) connecting two phenyl rings (Figure 2.1a). The most interesting character about azobenzene is the reversible photoisomerization between an extended *trans* (*E*) and a shorter *cis* (*Z*) isomer upon irradiation with different wavelengths or heating (Figure 2.1). Being completely reversible, this isomerization is known as one of the cleanest photoreactions, free from any side reactions.[49] Upon *trans* to *cis* isomerization, the distance between the 4 and 4´ positions of azobenzene reduces from 0.99 nm in the *trans* state to 0.55 nm in *cis* state. The intramolecular motion caused by the geometrical changes in azobenzene is very large by molecular standards and it is no surprise that azobenzene holds potential for constructing useful molecular machines.

The *trans* isomer is more stable,[50,51] and the isomerization barrier (energy to the cis- state) is on the order of 200 $kJmol^{-1}$.[52] Since the *trans* isomer is more stable, annealing can also convert the *cis* into the *trans* state. The potential energy landscape of azobenzene (Figure 2.1 b) has been determined in *ab initio* calculations and experimentally proven by spectroscopy. [52,53,54]

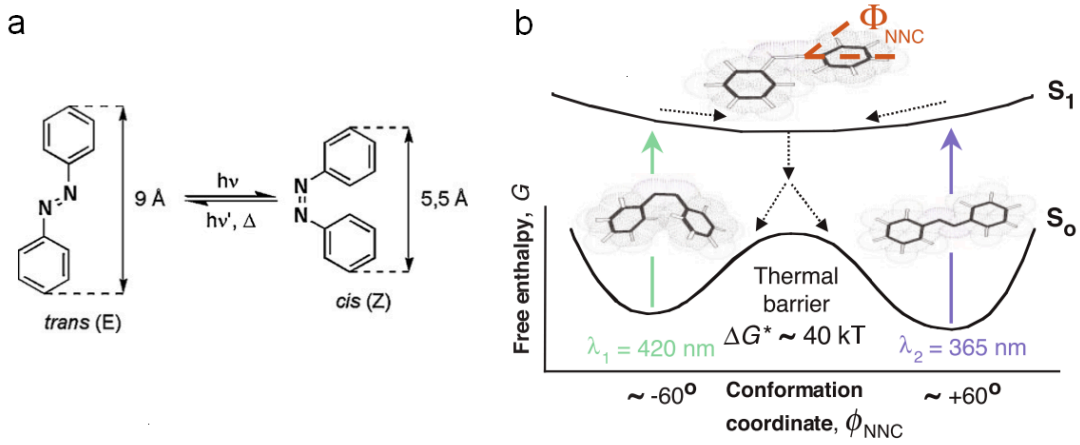

Figure 2.1 (a) Isomerization of azobenzene between *trans* and *cis* conformations upon irradiation or heating. (b) Schematic of the potential energy for the reversible azobenzene *cis-trans* transition along the inversion pathway. The *x* coordinate is the bond angle, Φ_{NNC}, which from the *cis* to the *trans* position changes the bond angle from about –60° to +60°. The transition can be induced by optical excitation from the singlet electronic ground state S_0 to the first excited singlet state S1 (*cis* form, λ_1 = 420 nm; *trans* form, λ_2 = 365 nm). [The shown graph is based on previous theoretical[52] and experimental[53,54] data]. Schematic taken from the Ref.[17]

2.1.2 Molecular motion of azobenzene

The mechanism of the molecular motion of azobenzene during isomerization has undergone considerable debate. It takes place either through a rotation of the N—N bond, with a ruptured π bond, or through inversion, with a semilinear and hybridized transition state formed in the excited state, where double bond (N=N) remains intact (Figure 2.2). Studies using picosecond Raman and femtosecond fluorescence spectroscopy show a double bond in the excited state, confirming the inversion mechanism.[55,56] In contrast, Ho *et al.* found evidence that the pathway is compound-specific.[57] In addition, the theoretical calculations indicate that energetically both pathways of rotation and inversion are possible, though the inversion

pathway is preferred.[58,59] Thus, both mechanisms may be occurring and the dominating pathway will be depending on the structure of the specific molecule and surroundings.

The inversion pathway is illustrated in Figure 2.1b, where the absorption of a photon in the *trans* absorption band will cause the *trans* isomer to convert to the *cis* isomer via a bond angle Φ_{NNC} change from +60° to -60° for an in-plane transition of the phenyl ring. The irradiation with a second wavelength (corresponding to the *cis* absorption band) can cause the back-conversion.

The inversion pathway requires less free volume in comparison to the rotation pathway. It has been estimated that successful isomerization via the inversion pathway requires only a free volume of 0.12 nm^3 versus approximately 0.38 nm^3 for the rotation pathway.[60,61] In general, the matrix constrained free volume could affect photochemical reactions of azobenzene and needs to be considered.[62] Nevertheless, the rather small free volume required for the inversion mechanism explains how isomerization of azobenzenes can take place even in rigid materials, such as glassy polymers.

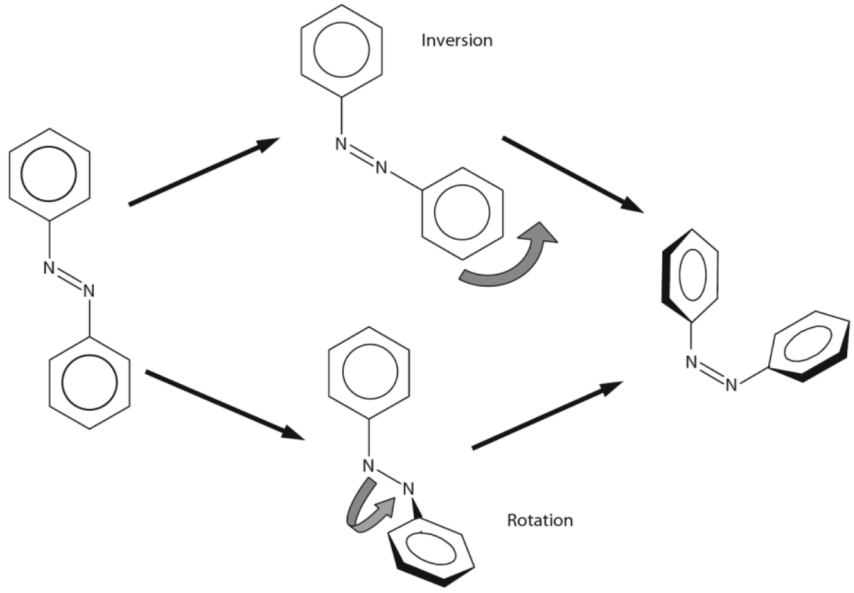

Figure 2.2 The mechanism of azobenzene isomerization proceeds either via rotation or inversion. The *cis* state has the phenyl rings tilted at 90° with respect to the CNNC plane. Schematic taken from the Ref.[63]

2.1.3 Determining the mechanical force of single azobenzene-containing polymers during isomerization

Molecular machines are able to exert forces or perform mechanical work. It is important, therefore, to be able to evaluate experimentally the optomechanical force on the single molecule level. In particular, Gaub's group has demonstrated a sophisticated experimental approach in this regard.[17] In this method, a freestanding strand of a polymer incorporating azobenzenes in the backbone has been covalently bounded between a SFM cantilever and a glass surface (Figure 2.3). The all-*E* polymer was isomerized by pulses of UV laser light, causing the polymer strand to contract as seen by the bending of the SFM cantilever towards the glass side. This proves that individual azobenzenes can isomerize against the external force exerted by the SFM tip. Then the exerted force of the SFM tip could be eased by *cis-trans* isomerization with visible laser

light pulses and therefore, a complete optomechanical cycle on the single molecule level was demonstrated. It was found that optical *trans-cis* isomerization could only be prevented at an external force above 500 pN. This shows the ability to activate and power molecular-level devices by using light, which is attractive since it overcomes limitations such as diffusion or wiring.

However, in this experiment, the maximum conversion efficiency of photomechanical energy was estimated to be around 10%, a number that is to be improved by, for example, high-density configurations, i.e., approaching larger photodeformation of individual molecules.

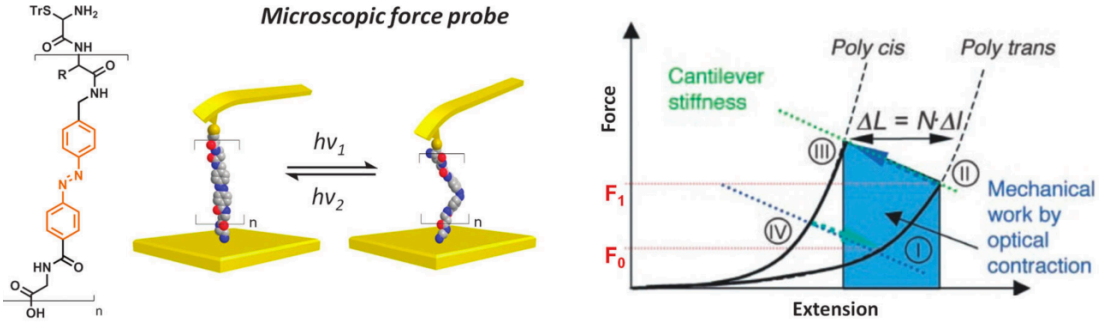

Figure 2.3 Measuring the mechanical force of azobenzene photoswitches by using single-molecule force spectroscopy. An azobenzene-containing polymer is stretched between a SFM tip and a glass slide; upon UV-irradiation, the individual polymer strand contracts and consequently bends the tip, thus delivering mechanical work. The optical *trans* to *cis* isomerization could only be prevented at an external force above 500 pN. The polymer was driven in a periodic mode, showing optomechanical energy eonversion in a single-molecule device. Schematic taken from the Ref.[17,48]

2.1.4 Designing larger photodeformation of individual molecules

Designing molecular architectures with larger photodeformation is a crucial step toward more efficient optomechanical devices in the future. Approaches to maximize photodeformation,[48] *i.e*. maximizing the geometrical changes, have been presented by incorporating azobenzene photoswitches into various molecular architectures. For example, one approach of incorporating azobenzene photoswitches in dendrimers has shown large changes of the hydrodynamic volume in solution (Figure 2.4).[64] In the studies,[21–23,65] the changes in hydrodynamic volume depend on how azobenzene photoswitches are incorporated, and on the rigidity of the dendrimers. Multiple azobenzenes at the periphery of the dendrimer or just one azobenzene at the core of a flexible dendrimer demonstrate rather moderate decrease in the hydrodynamic volume (ΔV_h = 12% for **D1**), but when three azobenzenes are incorporated in the core of the dendrimer, a significant decrease in the hydrodynamic volume (ΔV_h = 29%) was observed. The group of Müllen demonstrated that the more rigid dendrimers could generate larger photodeformations. [66]

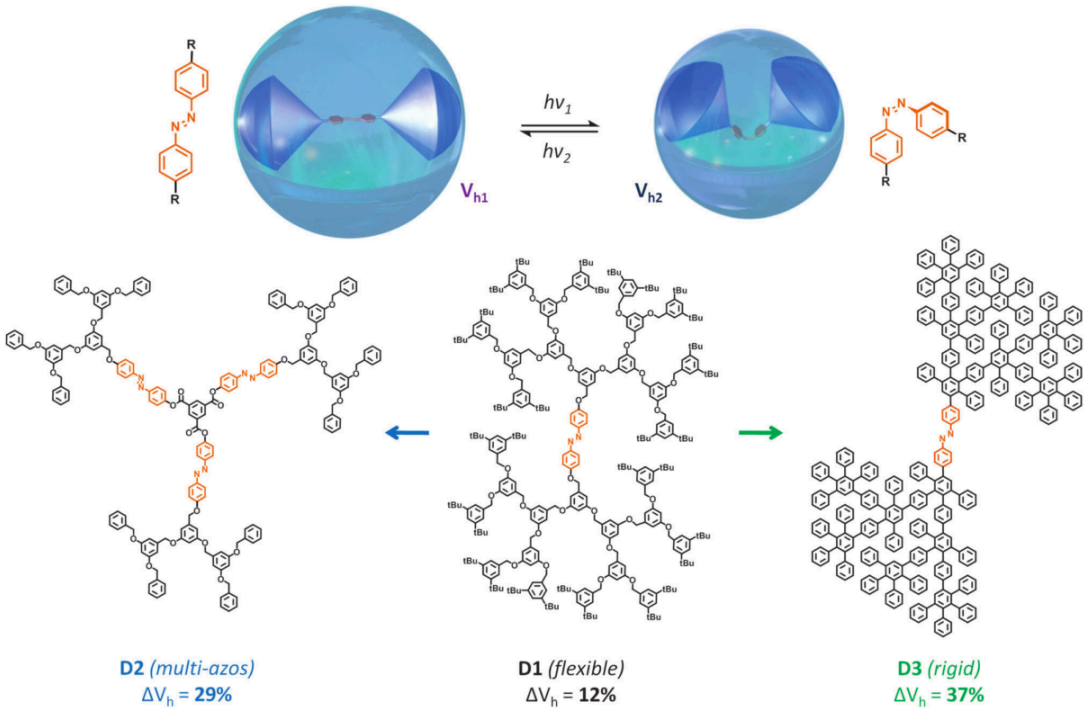

Figure 2.4 Photodeformation of a dendrimer. Incorporating only one azobenzene in the core of a flexible dendrimer demonstrates rather moderate decrease in the hydrodynamic volume (ΔV_h = 12% for **D1**). The more rigid dendrimers (**D2**)[24] and (**D3**)[66] can achieve larger photodeformation (ΔV_h = 29% and ΔV_h = 37%, respectively). Schematic taken from Ref[48]

More recently, the group of Hecht has incorporated multiple azobenzene photoswitches into a linear rigid-rod polymer. More than 30 azobenzenes were incorporated in the backbone of the rigid rod polymer **P2** (Figure 2.5). Especially, large twist angles (Φ) between chromophores were introduced with strategically positioned methyl groups in order that two adjacent chromophores could be electronically decoupled (without electronic decoupling, bisazobenzenes display low switching efficiency of *cis* content (16%) in the photo-stationary state). [67] Upon UV-irradiation these rod-like polymers in solution experienced a rod—coil transition, as indicated by a large decrease (ΔV_h = 72%) in hydrodynamic volume.[25]

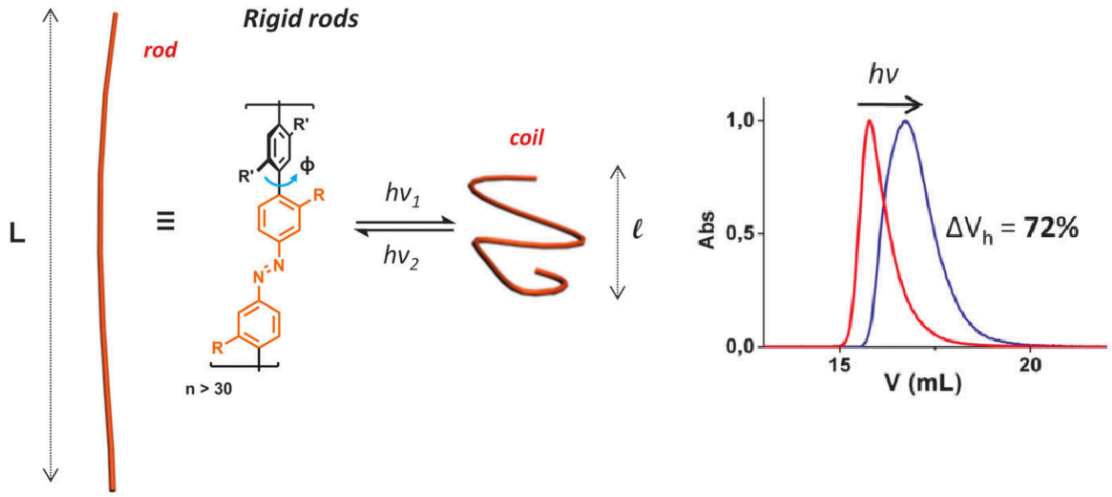

Figure 2.5 The rod—coil transition of the azobenzene-containing polymers (**P2**) can be induced reversibly by irradiation with UV and visible light. The conformational changes are reflected with a decrease in their hydrodynamic volume (V_h = 72%).[25] Schematic partly reproduced from the Ref[48].

The polymer **P1** investigated in this thesis is a homologue of **P2**. The detailed description and characterizations of **P1** are presented in Chapter 3.

2.2 Octadecylamine (ODA) modified graphite surface—a molecular workbench

In order to observe and investigate isolated single polymers on a surface, the surface needs to be chosen carefully. Here in this section I introduce the surface, which has been used in the experiments—octadecylamine (ODA) molecules tiling highly oriented pyrolytic graphite, HOPG.

In the early 1990's it was found that alkanes or alkyl chains containing amphiphiles could self-assemble into single layers of two-dimentional molecular patterns on the graphite surface.[68–71] These single molecular layers that modify the graphite surface and provide well-defined molecular environments constitute a "molecular

workbench", which can be utilized to modify and control the interaction between the substrate and adsorbed macromolecules.[72] By employing surface microscopy such as scanning force microscope (SFM), the macromolecules can be visualized and also manipulated by the tip of SFM cantilever.

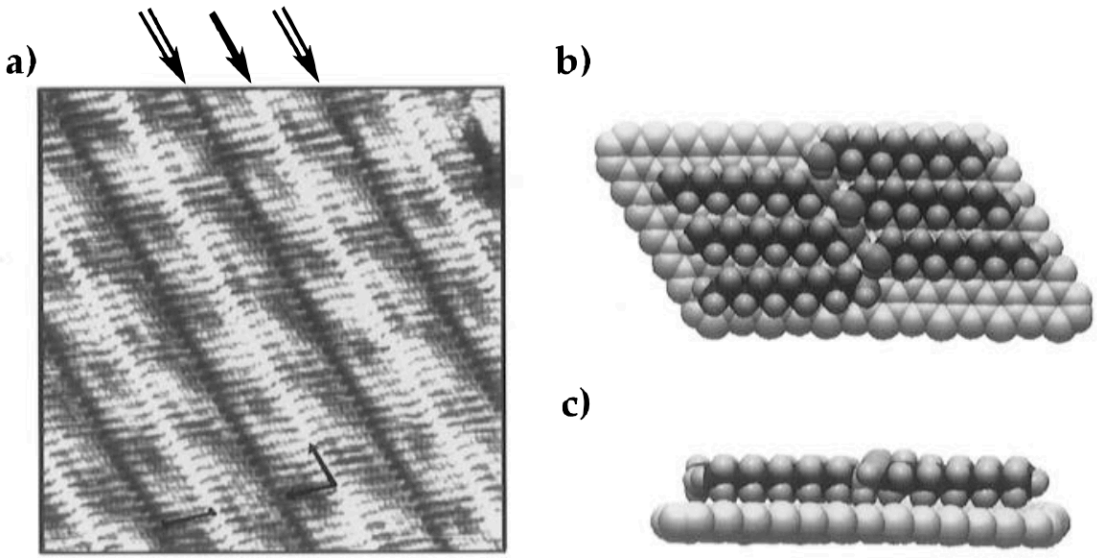

Figure 2.6 (a) An STM image of 1-octadecylamine ($CH_3(CH2)_{17}NH_2$) at the phenyloctane-graphite interface. Black bar indicates one molecular length. Presuming the bright ends being the NH_2 groups (indicated by →); they orient parallel to each other and paired in a "head to head" orientation. The ends of the alkyl chains appear as dark troughs (indicated by ⇒). (b) Top view of computer-generated model of an ODA film on a graphite substrate. (c) Side view of the model, showing that the lone pair of the amine N atom points out of the film in this structure. Images taken from Ref.[73]

Cyr *et al*. investigated the 2-D patterns of ODA on graphite by STM with atomic resolution (Figure 2.6a).[73] It is clearly seen that the 2-D lamellar crystalline film of ODA orients in well-ordered rows. The ODA molecules are lying flat and fully extended, as indicated by the length of one molecule coinciding with the theoretical all-*trans* length. Presuming the bright ends being the NH_2 groups; they orient parallel to each other and pair in a "head to head" orientation, which is attributed to hydrogen bonding. The hydrogen-bonding network of amine groups can be formed in a nonpolar solvent and it determines the molecular orientation within the monolayer. A computer-generated model with these observations in presented in Figure 2.6b.

The image of Figure 2.6a also displays a moiré pattern, which has been attributed to a molecular film that is incommensurate with the underlying graphite lattice. The Moiré pattern occurring here indicates that the intermolecular interactions between ODA molecules within the monolayer are stronger than between the molecule and the surface.

Octadecylamine molecules tiling HOPG have been utilized as a molecular workbench for the investigation of single macromolecules such as polyelectrolytes and DNAs. In particular, utilizing the electrostatic interaction, a negatively charged polyelectrolyte[74,75] adsorbed strongly to the positively charged amine head group of ODA, forming straight polymer segments, while the free polymer will normally behave as a worm-like chain. The aligning and straightening effect can also be observed on DNA deposited upon ODA surface.[76] Besides the electrostatic interaction, the adsorption of DNA on ODA lamellae could have more interactions involved, such as hydrophobic interaction or H-bonds formation.[76]

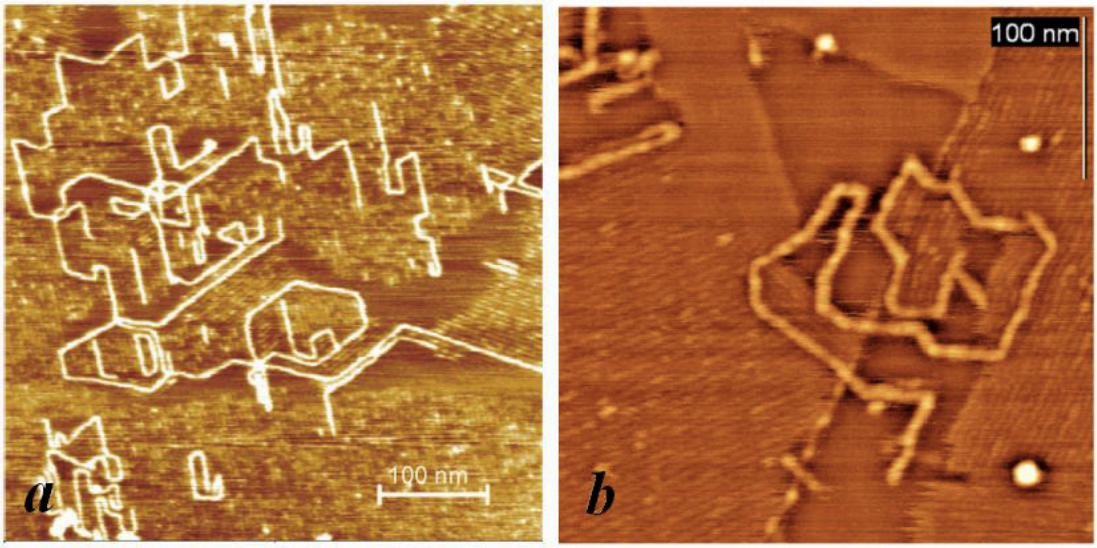

Figure 2.7 (a) SFM image of poly(sodium 4-styrenesulfonate) oriented on the surface of graphite covered with an ODA monolayer. Image taken from Ref.[75] (b) SFM images of DNA molecules, immobilized onto ODA modified HOPG. Image taken from Ref.[76] Both macromolecules and lamellae can be readily visualized with tapping mode SFM.

Chapter 3

Materials and Experimental Setups

3.1 Polymer P1 and its characterization in solution

3.1.1 Chemical structure of P1 polymers

The rigid-rod polymer **P1** (Figure 3.1)[25] which contains multiple azobenzene photoswitches in the backbone functionalized with dodecyl solubilizing groups, has been recently prepared by Suzuki polycondensation and characterized in solution.[25] Large twist angles were introduced between the chromophores to break the conjugation of the π-system.[67] This electronic decoupling leads to a relatively high *cis* content in the polymeric backbone (81% upon UV light (360 nm) irradiation in solution).[25] The molecular weight of the sample used in this study is $M_n \approx 40\,000$ g/mol with a polydispersity index of 1.7.[77] The estimated degree of polymerization is 15 and with a 2.4 nm long repeat unit, the estimated average length is >35 nm. The width of **P1** determined by the dodecyl chains (assumed stretched) is ~3.3 nm and its height determined by the methyl groups attached to the azobenzene moieties is $d_{methyl\text{-}methyl} \sim 0.5$ nm.

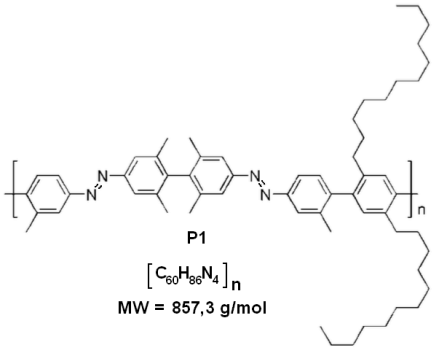

	M_n (g/mol)	M_w/M_n	Estimated DP_n*	Estimated average length* (nm)
P1	40 000	1.7	15	> 35

Figure 3.1 Chemical structure of **P1** and its characterizations

3.1.2 Characterization of P1 polymers in solution

P1 polymers in solution have been previously investigated by Bléger *et al.*[25]

3.1.2.1 UV-Vis absorption spectroscopy

UV-Vis absorption spectroscopy was performed in order to observe the photoisomerization of **P1** polymer in solution. Upon UV irradiation, the absorption band (300 nm—400 nm) of *trans* azobenzene in **P1** decreases while the *cis*-band (420 nm—480nm) increases during the transition of **P1** polymers from the *trans*-rich state to a *cis*-rich state upon UV irradiation (Figure 3.2). This result proves the ability of **P1** to undergo photoisomerization in solution.

The back transition from *cis*-rich to *trans*-rich upon 410 nm cut-off irradiation shows the isomerization is not fully reversible. As indicated by the spectrum (Figure 3.2b), the system is unable to recover completely back to the state before UV irradiation, which is possibly due to an increased steric hindrance, lack of free volume inside the *cis*-rich **P1** polymer, and the fact that *trans* azobenzene also absorbs light in the 400—500 nm region.

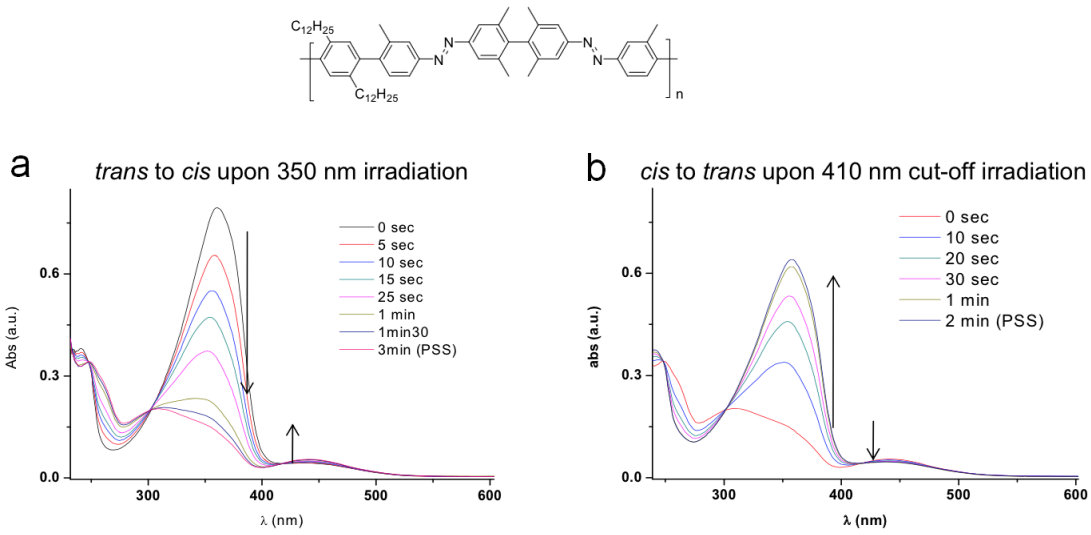

Figure 3.2 (a) Absorption spectra of a solution of **P1** in CH_2Cl_2 upon UV irradiation (365 nm) and the photostationary state (PSS) was reached in 3 minutes. (b) The back transition from *cis*-rich to *trans*-rich of **P1** upon 410 nm cut-off irradiation. The photostationary state was reached in 2 min.

3.1.2.2 NMR titration for determination of the *cis* content in the photo-stationary state (PSS)

The dramatic diminishing of the *trans* population is further checked by ^{1}H-NMR spectroscopy (Figure 3.3)[25]. The peaks assigned to the *E*-form (H_c, H_d and H_e peaks) diminished upon UV irradiation. The photo stationary state was reached when the NMR spectrum did not change further after 4 hours of irradiation. Comparing the integrations of H_c, H_d and H_e peaks (E-form) before and after irradiation allows for the determination of the PSS, where 81% overall Z content is determined.

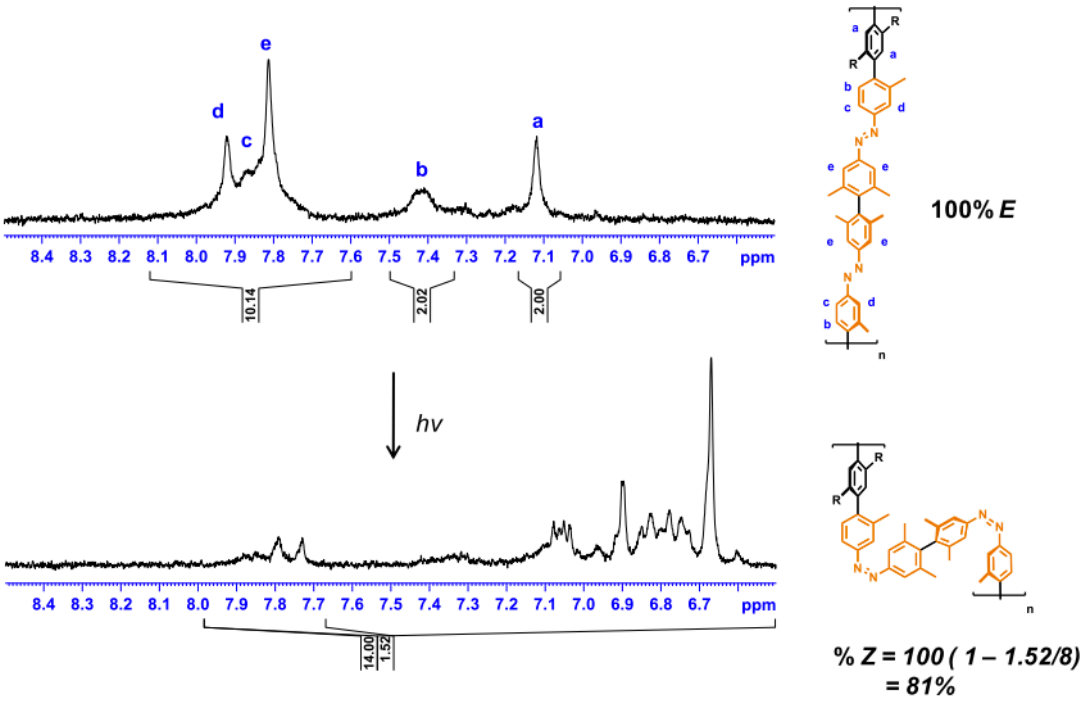

Figure3.3 ^{1}H-NMR spectra (aromatic region) of a 5 mg/mL solution of **P1** in CD_2Cl_2. Comparing the integrations of H_c, H_d and H_e peaks (E-form) before and after irradiation of 375 nm allows for the determination of the PSS; Figures taken from ref.[25].

3.1.2.3 Aggregation of P1 polymers in solution at high concentration

P1 polymers tend to form aggregates in apolar solvents at high concentration.[25] In Ref.[25] a high concentration (40 mg/mL) solution of **P1** in CD_2Cl_2 (*) was used. A broad peak in NMR centered on 6.2 ppm appears only in high concentration solution (Figure 3.4), and therefore, it is assigned to the aggregated areas. Ideally, the large twist angles (Φ,Φ') in **P1** should avoid their aggregation in solution, nevertheless, some attractive forces between **P1** polymers such van der Waals forces and π—π stacking may cause partial aggregation in high concentration solutions as sketched in Figure 3.4.

Interestingly, upon irradiation with 357 nm UV light, this broad peak of aggregation vanishes, which was attributed to the disruption of the aggregates.

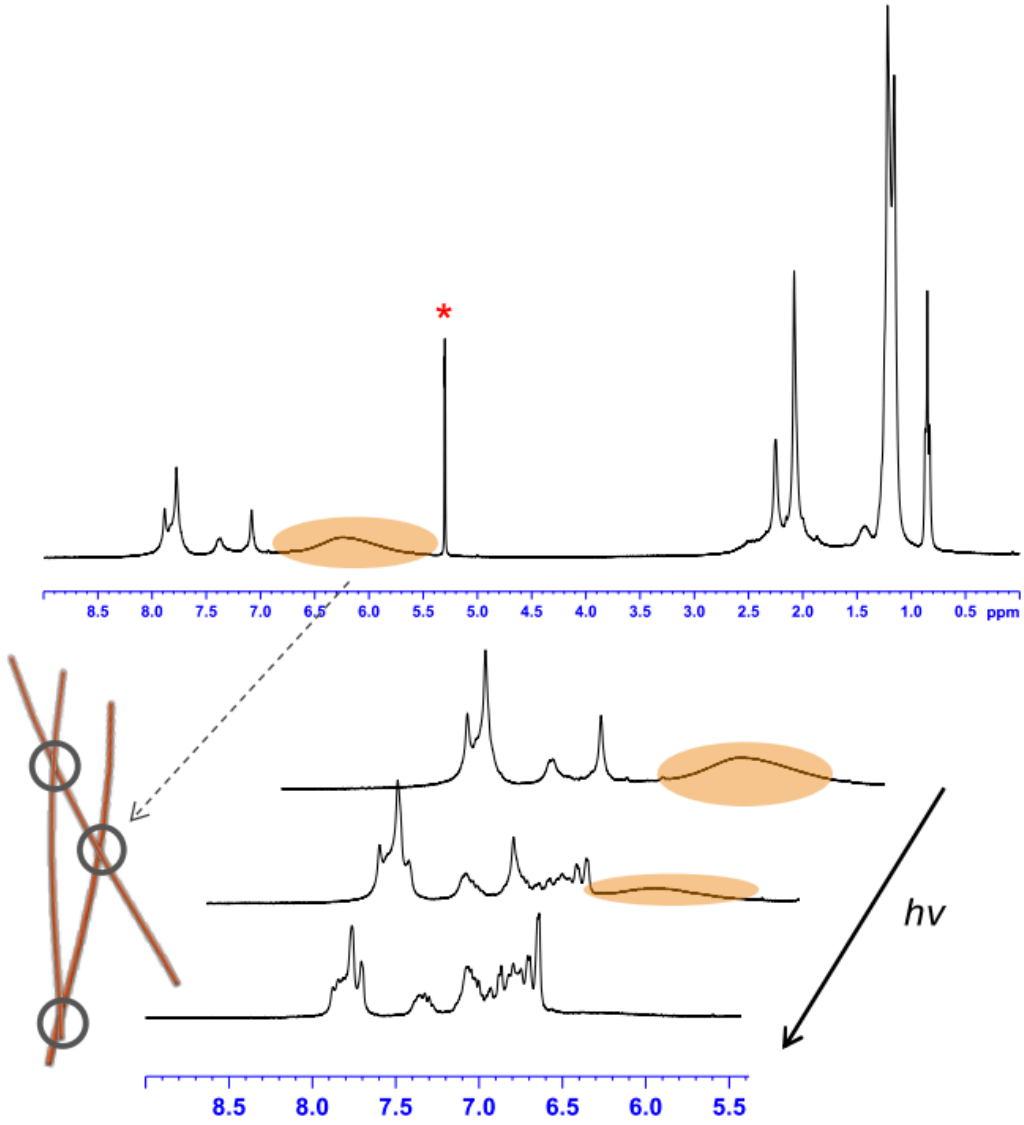

Figure 3.4 ^{1}H-NMR spectra of of **P1** in CD_2Cl_2 (*) with high concentration (40 mg/mL). A broad peak, centered on 6.2 ppm appears only in high concentration solution and is assigned to an aggregation peak, which vanishes upon irradiation with 357 nm UV light. It is attributed to the disruption of the aggregates. Figures taken from Ref.[25].

3.1.2.4 Disruption—reaggregtion cycle examined by scanning force microscopy (SFM) experiment

The light-induced disruption and reaggregation of **P1** aggregates in solution were further examined by SFM experiment (Fig 3.5). A **P1** solution (1 gL^{-1}) in THF was irradiated with UV light *ex-situ* for 10 min and 40 min, respectively, and flowingly spin-coated onto mica surface. The sphere-like aggregates decreased in size from around 80 nm height (without UV irradiation) to approximately 3 nm height (10 min of irradiation, see inset), which was attributed to less extended (*trans*-rich) **P1** polymers (see Figure 3.5b). The sphere-like aggregates re-appeared again after a few minutes of irradiating visible light (>400 nm), indicating the disruption—reaggregation cycle is reversible.

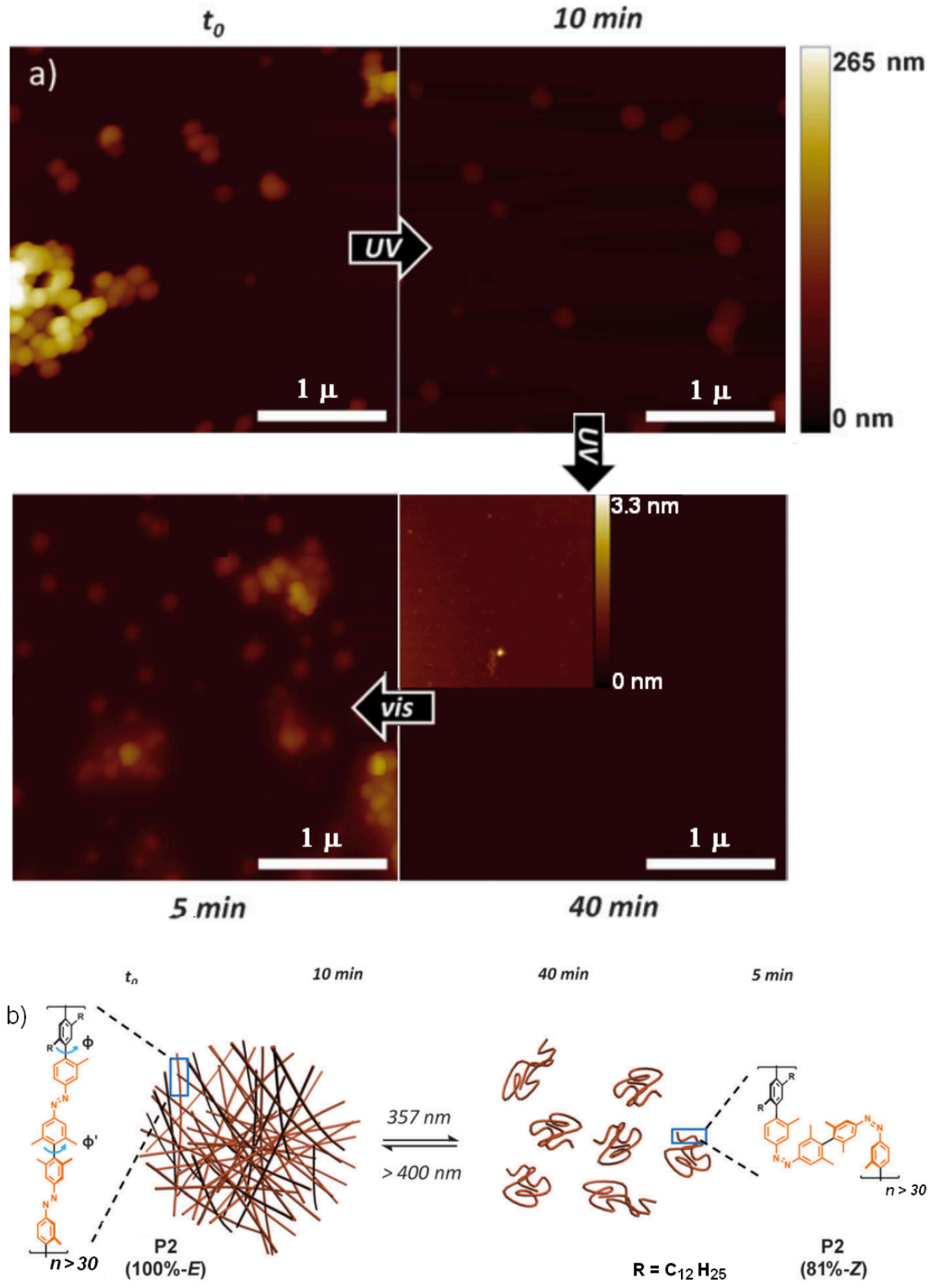

Figure 3.5 a) SFM snapshots of **P1** sphere-like aggregates deposited from solution onto a mica surface. After *ex-situ* UV irradiation for 10 min and 40 min, respectively, the size of aggregates decreased from around 80 nm height to approximately 3 nm height (see inset), indicating a disruption process of the aggregates. The sphere-like aggregates were observed again after a few minutes of *ex-situ* irradiation with the visible light (>400 nm). b) The sketch of **P1** polymer in the extended (100%-*E*) state forming sphere-like aggregates. The **P1** aggregates are disrupted in the *cis* rich (81 %-*Z*) state. Images taken from ref. [25].

3.2 Sample preparations and experimental setup

3.2.1 Sample preparation

In order to isolate single rod-like **P1** polymers, the graphite surface has been modified with a self-assembled monolayer (SAM) of octadecylamine (ODA). As previously demonstrated, this surface allows to isolate and orient single macromolecules such as DNA and polyelectrolytes.[74,75] First, octadecylamine (0.1 g/L in chloroform) was spin coated onto freshly cleaved HOPG (ZYH grade, Materials Quartz, Inc.) at 40 rounds per second. The resulting SAM was equilibrated in water: a droplet of Milli-Q water was deposited on the surface for 15 s and removed by spinning it off. SFM images of the ODA SAM reveal a lamellar structure with a width of $w = 6 \pm 0.2$ nm (Figure 3.6).

In a second step, **P1** (in dichloromethane) was spin coated onto the ODA monolayer. The sample was then stored in ambient conditions (white light) to allow the polymers to reach the equilibrium with the ODA monolayer.

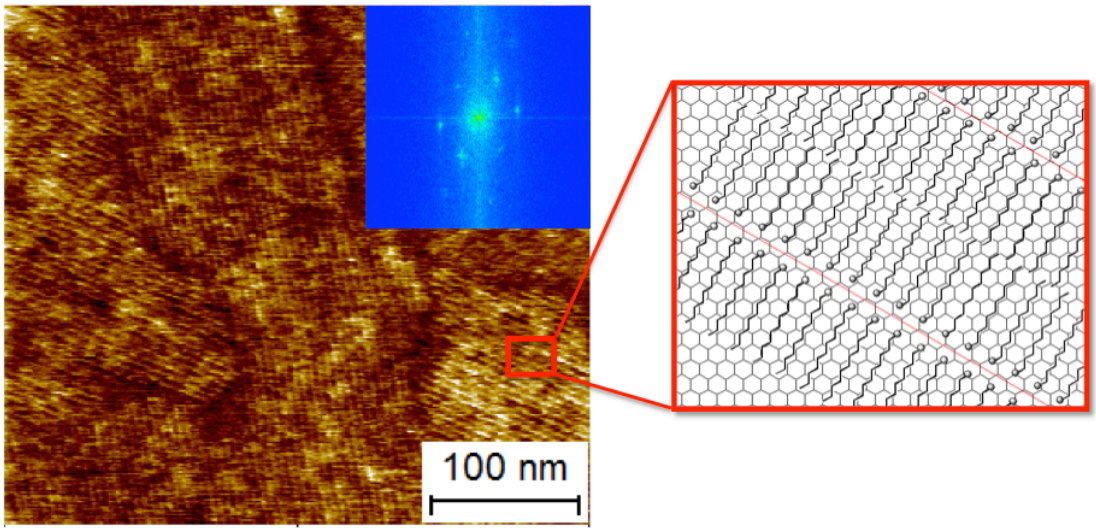

Figure 3.6 SFM image of ODA self-assembled monolayer on HOPG, showing 3-fold symmetric lamellar ODA domains with average lamellar width of $w = 6 \pm 0.2$ nm. Its fast Fourier transformation in inset reflects 3-fold symmetry. The schematic on the right shows the structure of the ODA monolayer on the graphite surface. The small circles denote the headgroups of amine.

3.2.2 Experimental setups

3.2.2.1 SFM measurements

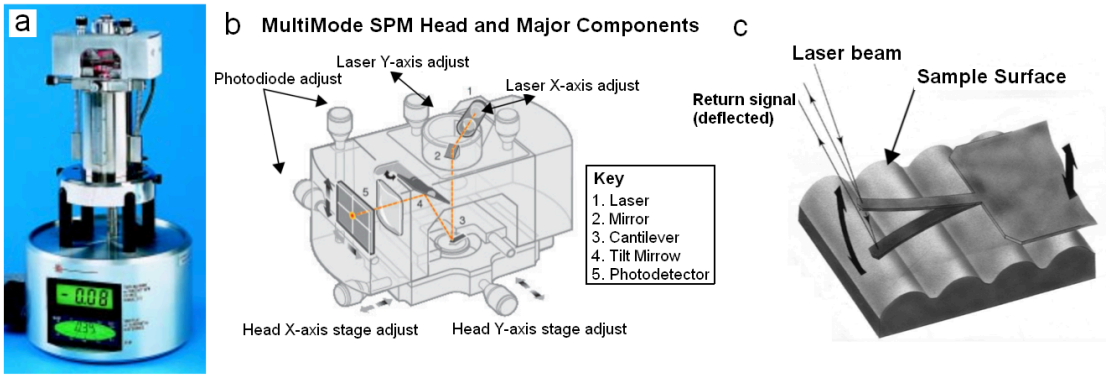

Figure 3.7 (a) The MultiMode microscope (Digital Instruments Inc., Santa Barbara, CA) includes an optical detection head, scanner, and microscope base. (b) MultiMode SPM head and Major components (c) Tapping cantilever on sample surface.

Imaging was performed by SFM using a multimode head (Digital Instruments Inc., Santa Barbara, CA) as shown in Figure 3.7a,b. The experiment was performed in tapping mode (Figure 3.7c). The cantilevers used were silicon Olympus microcantilevers (Figure 3.8) with a resonance frequency of 70 kHz and a spring constant of 2 N/m. The small spring constant is particularly suitable for soft samples. The apex of the tip is ideally point terminated; yet an effective finite apex radius between 7 nm to 15 nm needs to be considered in actual calculations.[78]

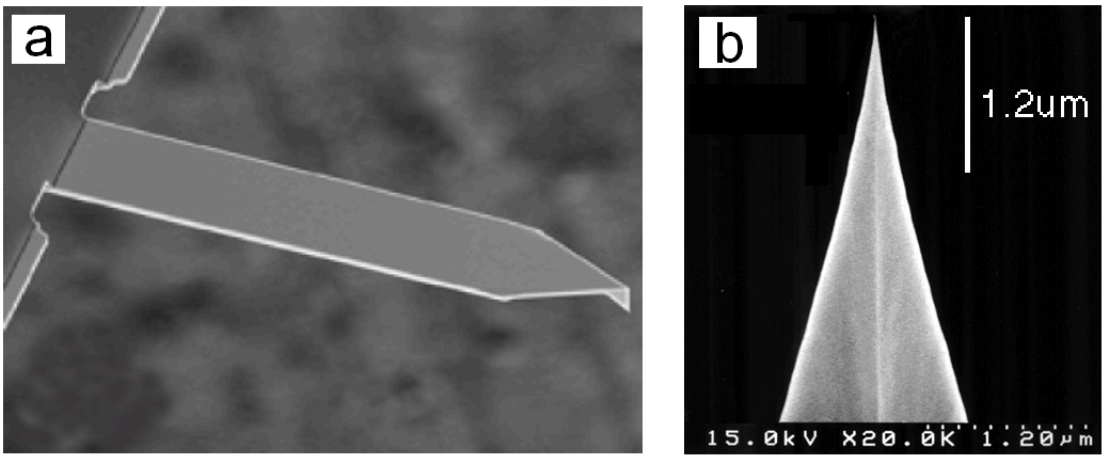

Figure 3.8 (a) Picture of a silicon Olympus microcantilevers. (b) SEM picture of a tetrahedral tip observed from the side of a cantilever, showing sharp effect around tip top.

3.2.2.2 Light sources

For *trans* → *cis* photoisomerization of **P1** polymers on the surface, a LED UV light source (Nitride Semiconductors Co., Ltd. see Figure 3.9a) was used in order to easily project UV light onto the polymers on surface. The estimated intensity is $I \approx 150$ W/cm^2. The output spectrum of UVlight (Figure 3.9 a) shows a clean peak output centered around 365 ± 10 nm, which is within the *trans* band of the **P1** polymer. The UV light indeed triggers *trans* to *cis* photoisomerization of **P1** polymers in dichloromethane (concentration 1g/L in 0.1 mm cuvette) as indicated by a decreased *trans* band and an increased *cis* band (Figure 3.9b); the same behavior has previously been shown in Figure 3.2a.

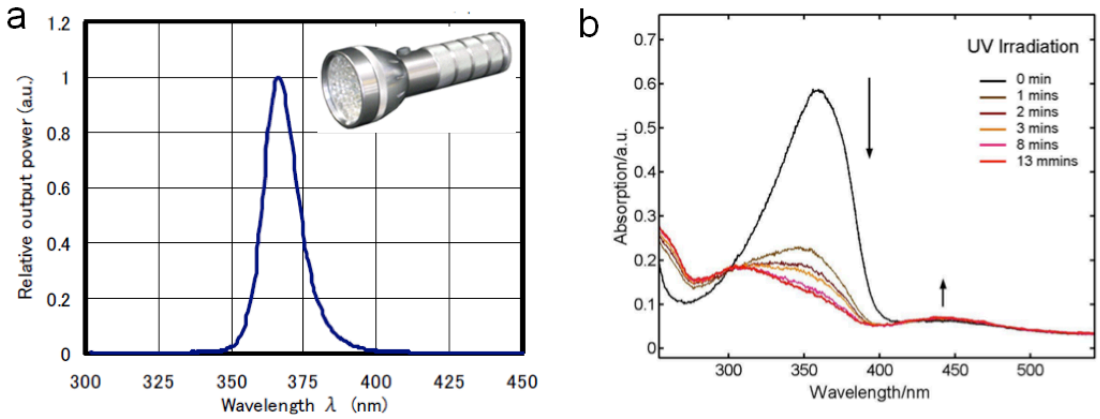

Figure 3.9 (a) Relative output power vs wavelength of UV light (365 ± 10 nm, LED flash light, Nitride Semiconductors Co., Ltd.) shows a clean peak centered at 365 nm. (b) Time evolution of the absorption spectrum of **P1** polymers in CH_2Cl_2 upon irradiation with UV light shown in (a).

For the *cis* → *trans* photoisomerization of **P1** polymers on the surface, I used the blue light at 436 ± 5 nm from a mercury lamp, Carl Zeiss HBO 50 (Figure 3.10a). The output at wavelengths other than 436 ± 5 nm were efficiently blocked by the filter (AHF Analysentechnik F27-436, see Figure 3.10). The intensity of the blue light is estimated to be $I \approx 40$ mW/cm^2.

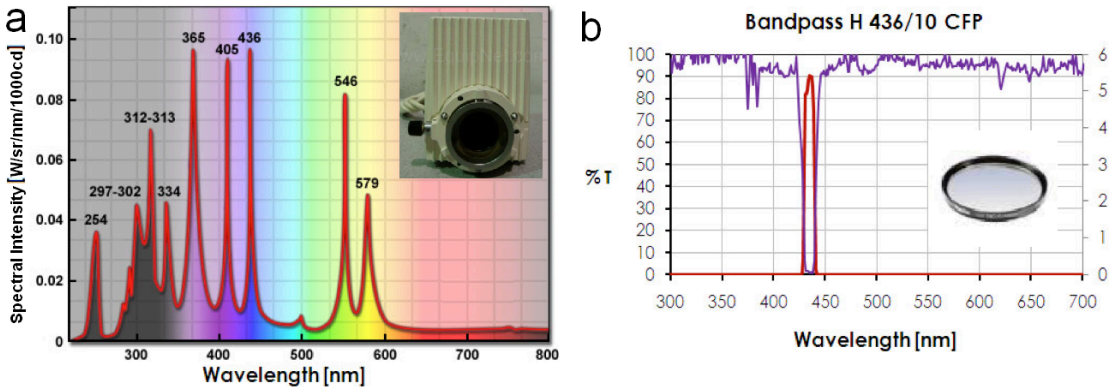

Figure 3.10 (a) Spectral intensity of a mercury lamp, Carl Zeiss HBO 50 with sharp blue light centered around 436 nm. (b) The transmittance of a 436 nm filter that is used to allow only blue light of 436 nm passing by.

The incident light was guided and focused onto the sample surface at 45° incident angle (Figure 3.11), generating a light spot of 1 cm diameter on the sample. During irradiation, the cantilever was lifted up to avoid blocking the incident light.

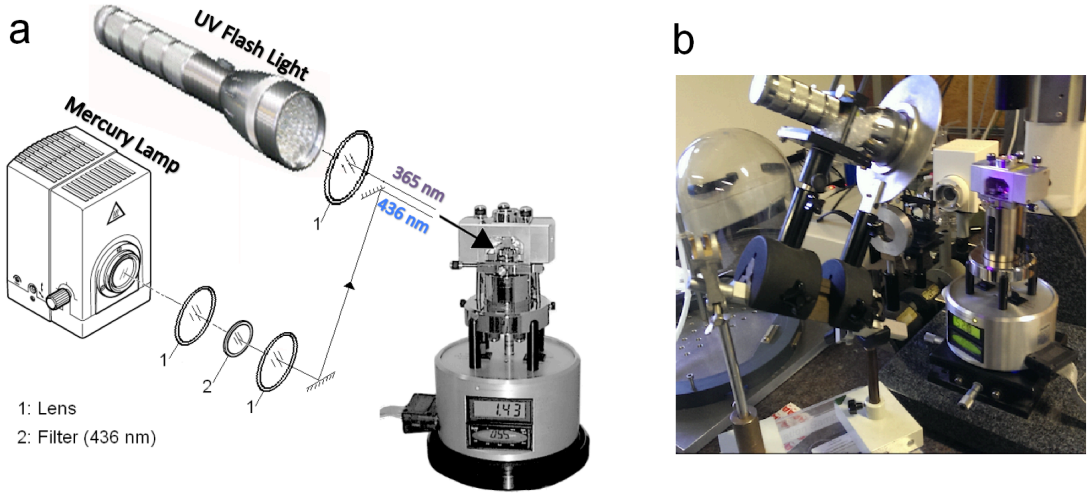

Figure 3.11 (a) Sketch of the incident UV light (365 nm) and blue light (436 nm) guided and focused onto the sample surface at 45° incident angle. (b) Picture of experimental setup.

Chapter 4

Results and Discussion

4.1 Alignments of rod-like azobenzene-containing polymers on nano-rows of amphiphiles

4.1.1 Introduction

Controlled alignment of single macromolecules on a solid substrate is a key challenge in nanoscience. Many studies about alignments on the single macromolecular level were carried out by employing a so-called "molecular workbench", which consists of an atomically flat substrate, such as the basal plane of highly oriented pyrolytic graphite (HOPG), covered with a monolayer of molecules such as alkanes or amphiphilic hydrocarbons,[69,73] that interacts and orients the on-top adsorbed single macromolecules. Subsequently, both the molecular substrate and the aligned single macromolecules can be visualized and correlated by scanning force microscopy (SFM) at a resolution on the nanometer scale.

Octadecylamine (ODA) molecules tiling HOPG has been proven a good candidate for aligning macromolecules such as DNAs[74,76,79] and synthetic polyelectrolytes.[74,79] Negatively charged polyelectrolytes adsorb strongly to the positively charged amine head group of ODA, forming straight polymer segments parallel to the ODA lamellae. Besides the electrostatic interaction, the adsorption of DNA on ODA lamellae may involve more interactions, such as hydrophobic interactions or H-bonds formation.[76]

I investigated the alignments and morphologies of azobenzene-containing polymers **P1** (see Figure 4.1) at different surface coverage on ODA self-assembled on HOPG, and I observed the change from previously reported parallel alignment at high surface coverage to the both parallel and perpendicular alignment at lower surface coverage. Particularly, the perpendicular alignment of macromolecules on an ODA surface has not being reported before for polymers, such as polyelectrolytes or DNAs. I propose a model based on the hydrophobic interaction of alkyl side chains of the polymers with ODA surface to elucidate their alignments.

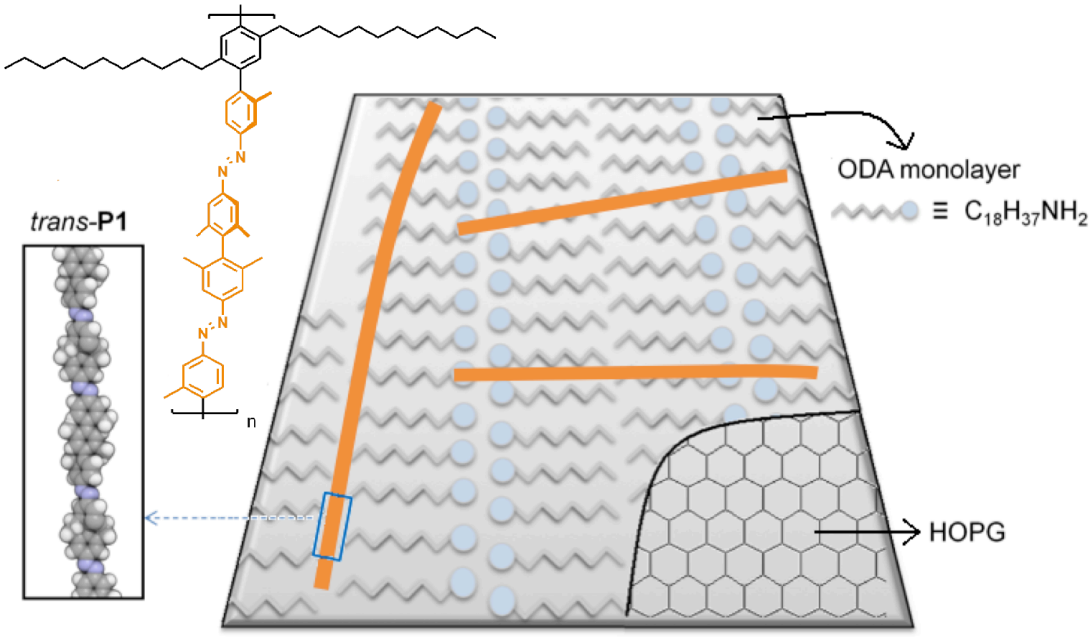

Figure 4.1 Chemical structure and schematic representation of **P1** in the extended (*trans*-rich) state on graphite modified with an octadecylamine (ODA) monolayer. Isolated single **P1** tends to align parallel or perpendicular to ODA's amphiphilic nano-rails.

4.1.2 Parallel and perpendicular alignments

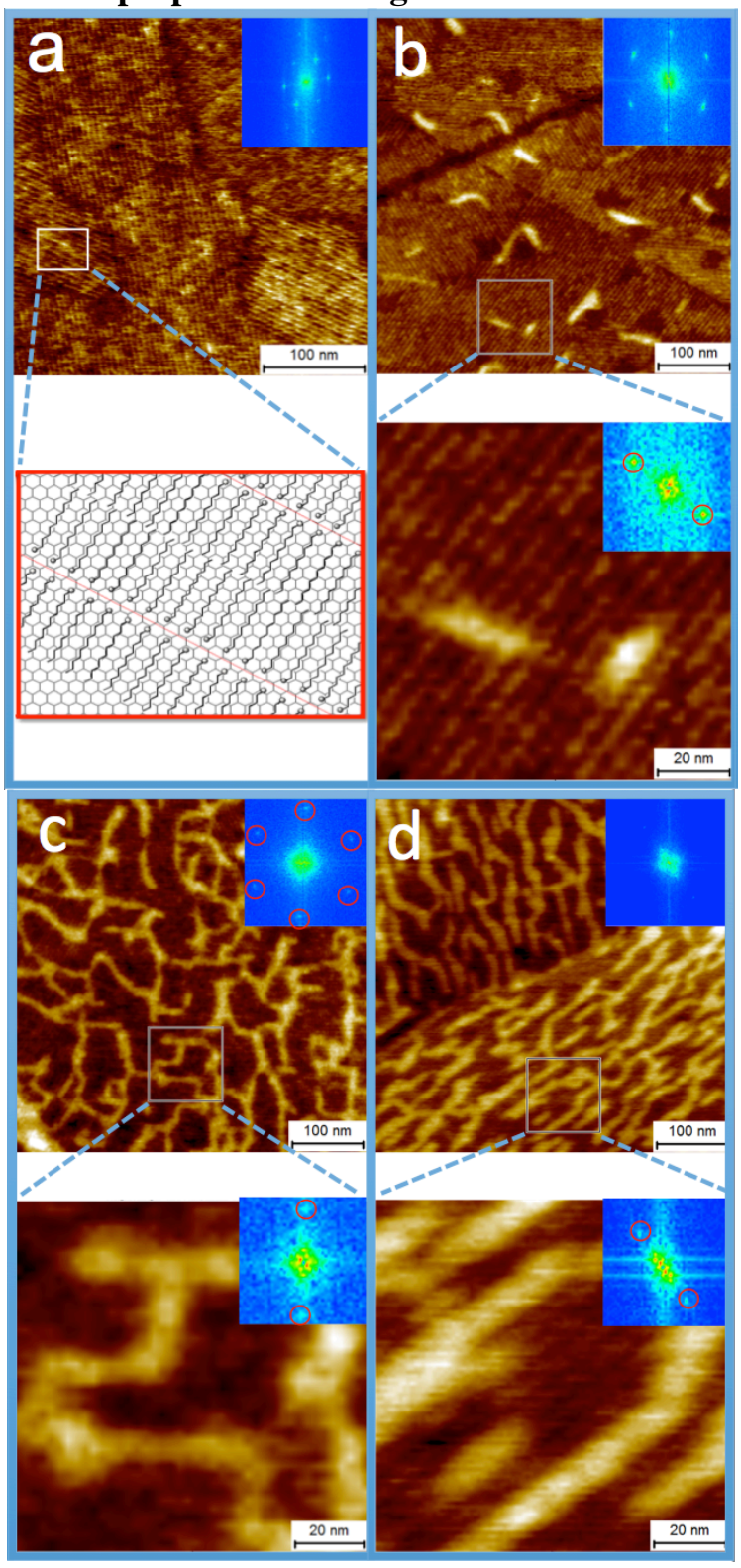

Figure 4.2 SFM topographic images of (a) ODA monolayer covering graphite surface (as illustrated by the sketch) and rod-like azo-polymers (**P1**) deposited on top of ODA monolayer with different surface coverage of (b) 4.5% (c) 35.3% (d) 49.5%. The zoom-in images (100nm×100nm) show that on single lamellar domain polymers are aligned parallel and quasi-perpendicular with respect to lamellae at lower surface coverage (b and c), and predominately parallel aligned at higher surface coverage

(d). The insets are fast Fourier transform (FTT), showing the signals of the lamellar pattern of ODA on graphite (indicated by red cycles for the easy seeing of eyes).

Figure 4.2(a) shows the SFM topographic image of an ODA monolayer with differently oriented domains covering a graphite surface. The ODA molecules in each lamellar domain orient in the same direction as illustrated by the sketch. The fast Fourier transform (FFT) in the inset shows six symmetric spots, reflecting three-fold symmetric alignments of ODA domains on the graphite surface. The subsequent deposition (spin coating) of **P1** solutions of different concentrations of 0.005 g/L, 0.2 g/L and 1 g/L onto an ODA monolayer results in 4.5% (b), 35.3% (c) and 49.5% (d) surface coverage, respectively. The FFT images in the insets of (b) and (c) show six symmetric spots, reflecting three-fold symmetric alignments of ODA domains on graphite. Due to the higher coverage of polymers in (d), the lamellae can only be seen in the zoomed-in image.

The zoomed-in images (100nm × 100nm) in Figure4.2 (b), (c) and (d) were selected from a single ODA domain (in which ODA molecules oriented in the same direction), showing both the polymers and the ODA lamellae underneath. The orientation of lamellae in a single ODA domain can be identified by symmetric pair signals in FFT (see insets). With only few higher protrusions, the deposited **P1** polymers in every surface coverage exhibit a rather thin sub-monolayer with an average height of 0.8±0.2 nm, which corresponds to the height of a single polymer. Such a homogenous height distribution suggests that the deposited polymers have sufficient time to rearrange during the evaporation of the solvent, thus avoiding the overlap of polymer chains.

Two categories of polymeric morphologies are found in the **P1** sub-monolayer, namely, polymeric ribbons and polymer rods. In low, 4.5%, surface coverage in (b), we observe mainly single rod-like polymers, whereas in high and middle surface coverage (c and d), mainly polymeric ribbons are observed. Notably in a previous study[25] it was observed that **P1** polymers in organic solvents will usually form spherical aggregates, which can be reversibly disrupted by alternating irradiation with UV and visible light. The SFM images here suggest that diluting the **P1** solution can also disrupt **P1** aggregates in a solvent.

Polymeric ribbons are generally wider and longer strips that connect to other polymeric strips or rods. In general, ribbons have apparent widths ranging from 10 nm to 22 nm, and apparent heights ranging from 0.7 nm to 1.6 nm. Based on the size of the ribbons that are longer and wider compared to single polymer rods and in some instances that two ribbons converge to one, we attribute such thin 2-dimentional polymeric ribbons to a few polymer chains lying flat parallel to one another with their dodecyl-side chains partially interdigitated. The large space (2.4 nm) between two dodecyl side chains alone the backbone of **P1** (Figure 4.1) should allow the insertion (or interdigitation) of dodecyl-chains from another polymer chain. Recent research[80] revels that a similar polymer designed with smaller space (1.4 nm) between two dodecyl-chains can interdigitate nicely their dodecyl side chains with neighboring polymer chains to form a zipper structure in the bulk.

The isolated polymer rods with an apparent width of ≈ 10 nm and height of ≈ 0.7 nm have been previously assigned to single **P1** polymers adopting rather stretched (*trans*-rich) backbones imaged with the same SFM tips.[26]

Interestingly, both polymer rods and ribbons seemed to align in certain directions related to the underlying ODA lamellae. At high surface coverage (d), both **P1** polymer ribbons align predominately parallel to the lamellae. At intermediate surface coverage (c), however, quasi-parallel and -perpendicular alignments of ribbons can be seen, exhibiting some sharp turns at angles around 90° (see zoomed-in image), which is different from previous reports of turning angles at 60° and 120°, reflecting the 3-fold symmetry of the underlying pattern. This 90° difference in alignments can be seen more clearly at low surface coverage (b), where single polymer rods align either parallel or quasi-perpendicular within a single ODA domain (see inset).

In order to find out which angles of **P1** polymer with ODA lamellae are present, a statistic analysis of the angle distribution was performed on single polymer rods at low surface coverage. The angles of 43 polymer rods related to lamellae were measured and presented from -45° to 135° with 5° intervals in Figure 4.3. Here, 0° represents the parallel alignment of the axis of the polymer rods to the underlying ODA lamellae, while 90° represents perpendicular alignment.

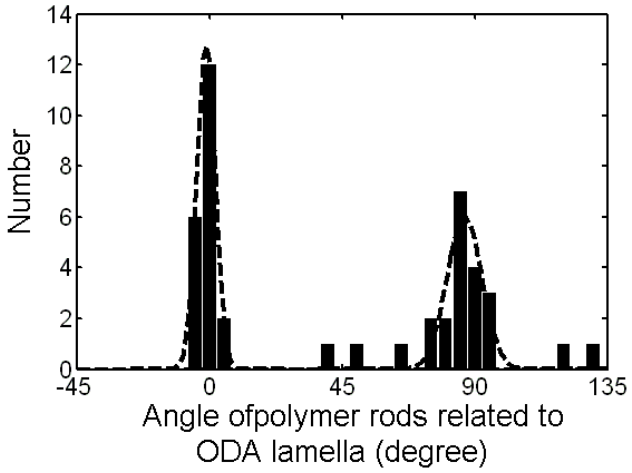

Figure 4.3 Number of **P1** polymer rods at different angles relative to ODA lamellae.

Figure 4.3 shows two dense populations of **P1** rods align around 0° and 90° that represent two regions of parallel and perpendicular alignments, respectively. Curve fitting (Gaussian) revels that the peak around 90° (FWHM =13.9°) is about twice broad as the peak around 0° (FWHM = 7.4°). Although there are few orientations of polymer **P1** rods beyond both regions of parallel and perpendicular alignments, 88 % of the polymer rods lie within these two regions.

To our knowledge, the perpendicular alignment of single macromolecules on an ODA surface has not been reported by previous studies of macromolecules, such as DNA or negatively charged polyelectrolytes that adsorb onto the positively charged amine groups in the ODA pattern, resulting in a solely parallel alignment.[79,74,76] Since **P1** polymers are electrically neutral, the alignment of the **P1** polymer on the ODA pattern should not be driven by electrostatics. After examining carefully the composition of the **P1** polymer, H-bond formation or π-π stacking interactions with the ODA pattern is also not likely. The remaining most possible interaction that contributes to the alignment is the hydrophobic interaction.

4.1.3 Modeling

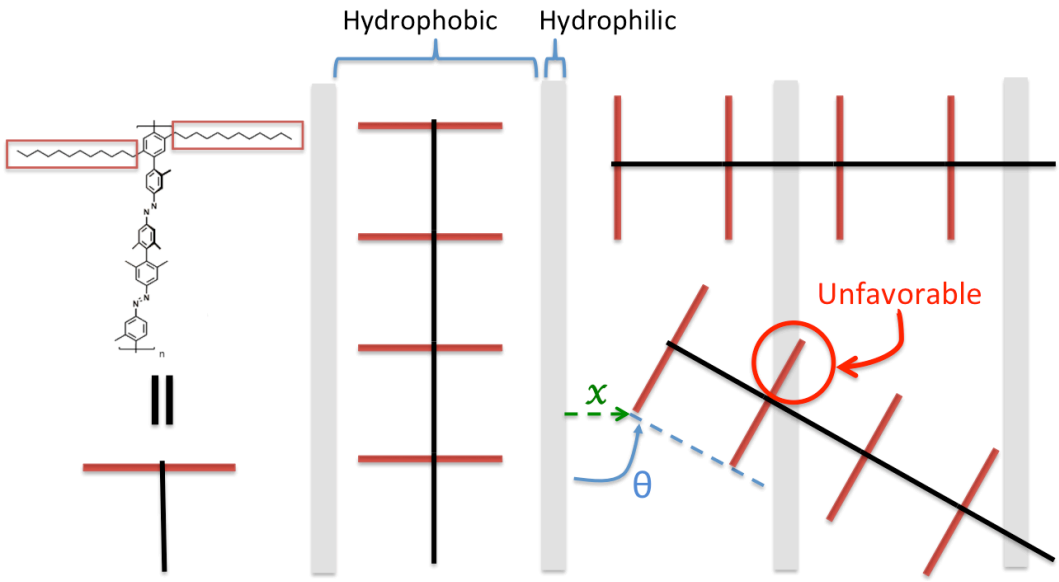

Figure 4.4 P1 polymer rod is represented by a straight black line (backbone) and a red line orthogonal to it (pair of dodecyl side chains) that prefer to align parallel or perpendicular to the amphiphilic "nano rows" of octadecylamine.

In the following I propose a model to understand how the hydrophobic interaction may contribute to the parallel and quasi-perpendicular alignments of **P1** polymer on ODA pattern. It is well known that ODA lamellae serve as amphiphilic nanoscopic "rows".[75,72,81] The hydrophilic rows of the amine headgroups, and the hydrophobic rows of the alkyl chains are represented by gray and white rows, respectively, in Figure 4.4. The backbone and the hydrophobic side chains of **P1** polymer rods are represented by black and red lines, respectively. I assume that the dodecyl side chains of the polymers are stretched so that all alkyl chains can adsorb on the underlying substrate to maximize the adsorption energy.[82]

In order to simplify the model further, I assume that the interaction of the backbone of **P1** with the ODA pattern is less important due to the bulky methyl groups and the large twist angle (Φ,Φ') between the chromophores that should reduces the direct contact of the backbone atoms with the surface. Therefore, I conclude that the dodecyl side chains play the critical role for the alignments I observed here.

The relevant variables in this model are the aligning angle (θ), the angle between the polymer's backbone and a hydrophilic row, and translational displacement x, i.e., the distance from a hydrophilic row to the left end of the polymer's first side chain, as sketched in Figure 4.4. The hydrophobic side chains of a polymer lying on the hydrophilic rows of ODA are considered energetically unfavorable. Such unfavorable contact is proportional to the total length of its side chains on the hydrophilic rows at a given θ and x. In order to minimize such unfavorable contact, polymer rods should optimize θ and x during deposition to have all their side chains on the hydrophobic rows. Therefore, the objective is to find all possible "zero-contact" angles θ_0, where all the side chains of a polymer rod have zero contact with hydrophilic rows.

With optimized x, the aligning angle $\theta = 0°$ could be one of the "zero-contact" angles where no side chains are on hydrophilic rows (see Figure 4.4). This is because the **P1** polymer has a narrower width (3.3 nm) than the hydrophobic row (4.64 nm). Along the same lines, the aligning angle $\theta = 90°$ is another zero-contact angle. This is because the width of a hydrophilic row (0.53 nm) is significantly smaller than a hydrophobic row (4.64 nm) of ODA on graphite. (For the mathematical formulae, see Appendix I).

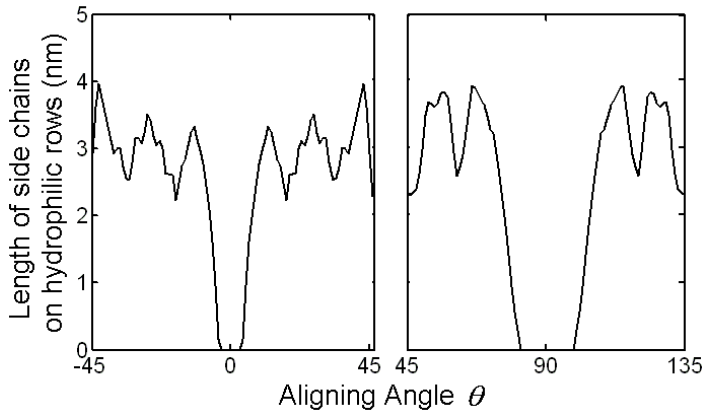

Figure 4.5 Calculated total length of unfavorable contacts at different aligning angles for a polymer rod with averaged length 22.5 nm (or ca. 9 repeat units)

Figure 4.5 shows the calculated sum length of side chains on hydrophilic rows at different aligning angles for a polymer rod of 22.5 nm length (an averaged length from our data) or 9 repeat units. The values of translational displacement x are optimized separately in the region (-45° to 45°) and in the region (45° to 135°) to insure that zero-contact angles θ_0 around 0° and 90° will be maximized. The result in Figure 4.5 shows the unfavorable contact of side chains on hydrophilic rows ranging from 2.3 nm to 4 nm could drop to zero around 0° (parallel alignment) and 90° (perpendicular alignment) and the possible zero-contact angles θ_0 are 6° (from -3° to 3°) and 18° (from 82° to 99°) in parallel and perpendicular regions, respectively. Therefore, this result shows not only perpendicular alignment is possible, but also suggests a rather broadened angle distribution around perpendicular alignment, which is in accordance with our experimental data in Figure 4.3.

However, this model cannot explain some few orientations of polymer **P1** rods beyond both parallel and perpendicular alignment in Figure 4.3. The possible reasons could be due to local surface defects in the ODA monolayer or a possible reorientation of amphiphile molecules in close vicinity of the polymer backbone that

cannot be resolved by SFM. The other possible reason could be due to rather speedy evaporation of the solvent from the polymer that leaves less time for polymer rods to orient to most favorable orientations. Actually, the real modeling should involve more complex calculations of the interactions of polymers with the underlying surface atoms as well as the kinetic during deposition should be considered, which is beyond the scope of this thesis. Nevertheless, the model provides a simple way to explain qualitatively both parallel and quasi-perpendicular alignments of polymers functionalized with alkyl side chains lying on the amphiphilic nano-rails.

The reason why mainly parallel alignments of polymer are observed at high surface coverage is probably that at higher density polymer-polymer interactions (such as interdigitation) start to play a bigger role than the polymer-substrate interaction.

4.1.4 Conclusion

Azobenzene-containing rod-like polymers functionalized with alkyl side chains have been deposited as single polymers from solution at different concentrations onto ODA monolayers on the basal plane of HOPG. At high surface coverage polymeric ribbons are dominant, whereas at low surface coverage single isolated rod-like polymers are observed with both, the unusual perpendicular and the more common parallel alignment of **P1**. A model based on the hydrophobic interaction of the side chains of the polymers with well-defined amphiphilic nano-rows can qualitatively explain both parallel and rather broadened perpendicular alignments, which should be taken into consideration for both study and development of bottom-up molecular systems including amphiphilic lamellar structures.

4.2 Light-induced contraction and extension of single macromolecules on a modified graphite surface

4.2.1 Introduction

Control over the motion of single molecules is a fundamental challenge in the field of nanotechnology, in particular for the development of artificial molecular machines[3,4,83] and typically requires to convert external energy—either chemical fuels or physical stimuli—into movement through concerted conformational changes. Ingenious systems have been developed, sometimes inspired by Nature, such as artificial muscles[8,15] and DNA/molecular walkers,[84–87] or by our macroscopic surrounding, like molecules resembling wheels,[88] pinions,[5] and even cars,[11,13,14] for which the most sophisticated example to date is a system equipped with four rotary motors fueled by electrons *via* voltage pulses.[89] Physical stimuli, which are particularly attractive as they allow for non-invasive control with typically high spatial precision, include electrons,[89–91] mechanical manipulation *via* the tip of a scanning probe microscope,[88,5] and light.[92]

In that context, molecules able to undergo reversible conformational changes leading to large contraction and extension of their structures are of potential great interest. Small molecules, such as azobenzene photoswitches,[93] usually exhibit contractions and extensions of low amplitudes due to their limited size,[39,41,43,44] while macromolecules are more promising for obtaining mechanical movements over larger distances.[16,17,48] Recently, Bléger *et al*. have shown that drastic contraction/extension cycles can be induced in solution on command in rigid-rod polymers incorporating

many azobenzene photoswitches in the main-chain (see **P1**, Figure 4.6).[25] The embedded photoswitches act as hinges, which upon light-induced isomerization lead to reversible shrinking and stretching of the polymer backbone. One key element of the molecular design is the rigidity of the backbone, in that case a poly(*para*-phenylene), which maximizes the photodeformation and should eventually allows for enabling large mechanical motion. Another crucial aspect of the design is the introduction of large twist angles between the azobenzene units in order to break the conjugation. This point ensures to attain a *trans*-rich photostationary state (PSS) upon irradiation with UV-light, since azobenzenes directly connected at their *para*-positions display rather *trans*-poor PSSs.[67] Rigid-rod polymers **P1** were shown to perform in solution, exhibiting conformational rigid-rod → random-coil transitions accompanied with changes in hydrodynamic volume of *ca*. 75%, as determined by static and dynamic light-scattering measurements. Nevertheless, in order for linear chains to eventually act as molecular machines, *i.e*. able to transport/manipulate other objects or perform mechanical work, they arguably have to be interfaced with robust scaffolds such as nanotubes, particles, or planar surfaces.[94]

In this section, we will present the immobilization and orientation of the photo-shrinkable linear polymer **P1** on a modified graphite surface, and provide a direct visualization of dramatic extensions, contractions, and crawling movements of single macromolecules induced by a physical, non-invasive stimulus, *i.e*. light.[95–97]A "molecular workbench" was employed, consisting of the graphene surface of highly oriented pyrolytic graphite (HOPG) covered by an ordered monolayer of flat lying octadecylamine (ODA), which has been used to both orient single macromolecules and manipulate them by scanning force microscopy (SFM) techniques.[79] Indeed, the

ODA monolayer decouples the polymers—both mechanically and electronically—from the surface, a point of prime importance since a strong mechanical coupling would prevent the polymers to move at all while an electronic coupling with the semi-metallic surface could impede the photoswitches to isomerize *via* fast quenching of the photo-induced excited-states.[98]

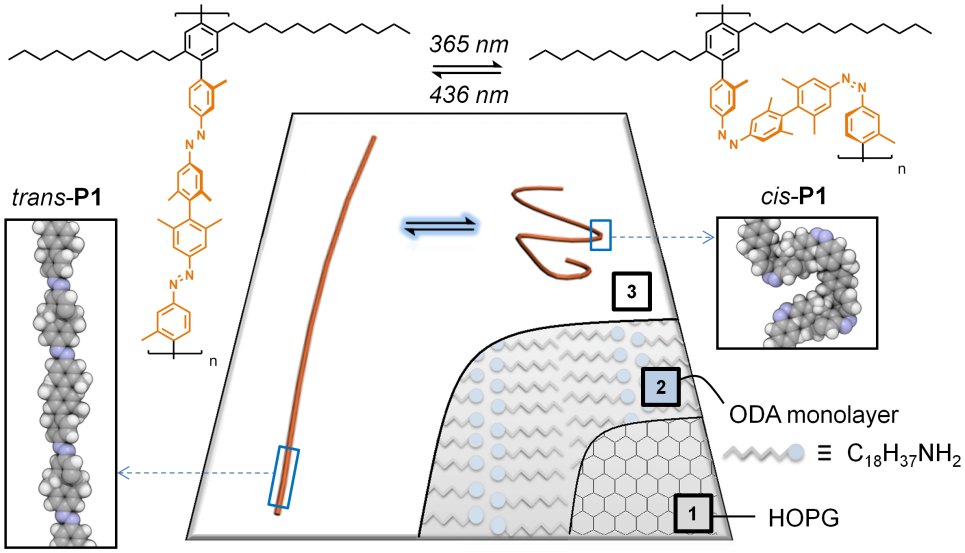

Figure 4.6 Chemical structure and schematic representation of **P1** in the extended (*trans*-rich) and contracted (*cis*-rich) state on graphite modified with an octadecylamine (ODA) monolayer. Isolated single **P1** can shrink and stretch upon exposure to UV (λ = 365 nm) and visible (λ = 436nm) light, respectively. The three layers are labeled: 1, HOPG; 2, ODA monolayer; 3, polymer **P1**.

4.2.2 Light-induced contraction of single polymers

4.2.2.1 Identifying single polymers on a surface

Rigid-rod polymers **P1** deposited on a graphite surface coated with an ODA monolayer were imaged by SFM (Figure 4.7a). Some rather high protruding defects serve as markers to ascertain that all SFM images were taken at the same location. Two different aligning directions with 60° orientation difference of the rod-like polymers **P1** mark a clear grain boundary at the top left corner, reflecting the 3-fold symmetry of the ODA lamellae under the **P1** polymers.[74,79] Many straight rod-like conformations confirm that the initial configuration of the polymer is *trans*-rich, as received from the synthesis and corresponding to the thermodynamically most stable form of azobenzene. Occasionally, some kinks within a chain as well as overlapping of different polymers were found, but overall **P1** macromolecules are aligned along the ODA lamellae located underneath. These lamellae serve as soft nanoscopic "rails", with the chemical nature of the hydrophilic head groups and the length of the alkyl chains defining a surface potential ripple, thus orienting the single polymer molecules on the surface.[79]

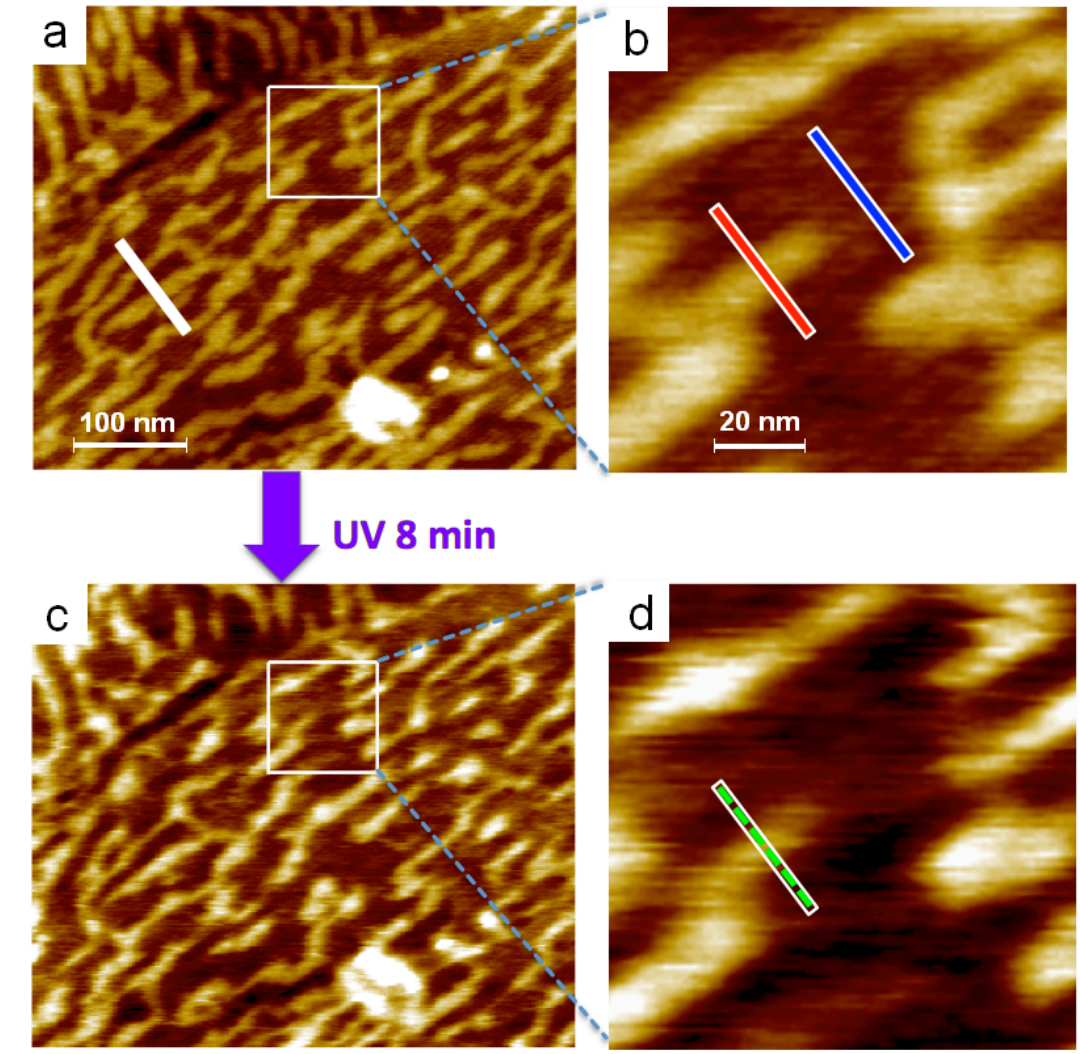
a
b
100 nm
20 nm
UV 8 min
c
d

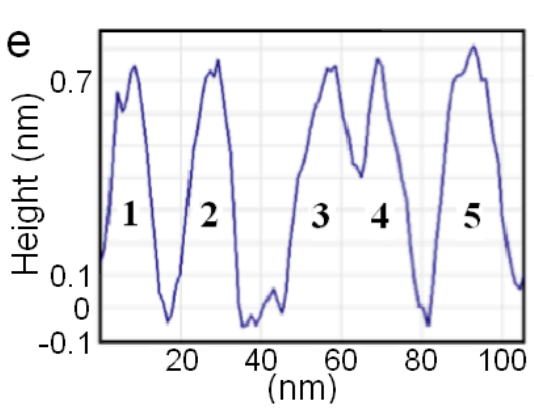
e
Height (nm)
0.7
0.1
0
-0.1
1
2
3
4
5
20
40
60
80
100
(nm)

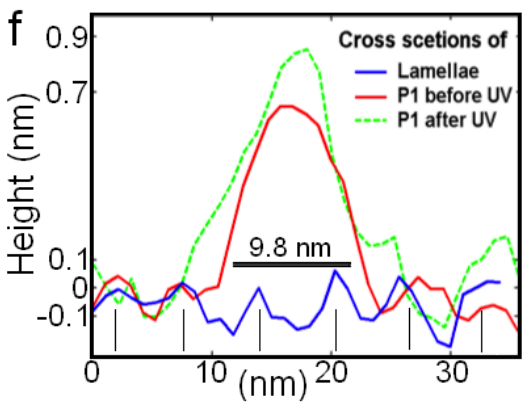
f
Height (nm)
0.9
0.7
0.1
0
-0.1
Cross scetions of
Lamellae
P1 before UV
P1 after UV
9.8 nm
0
10
20
30
(nm)

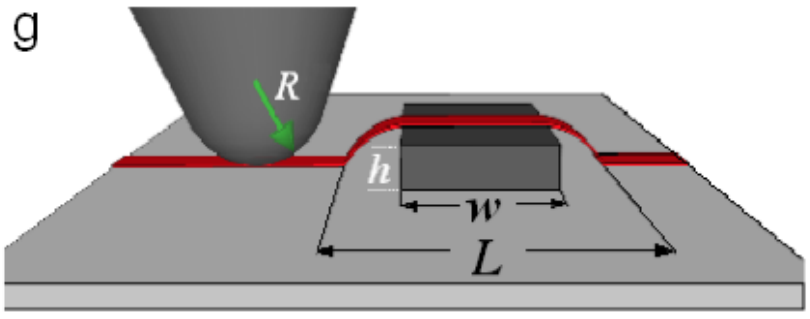
g
R
h
w
L

Figure 4.7 (a) SFM image of rod-like polymers **P1** aligned along ODA lamellae before UV irradiation. (b) Zoom-in image showing that the ODA lamellae were preserved post-deposition (width 6 ± 0.2 nm) with the rod-like polymers aligned along the axes of the lamellae. (c) SFM image of the same area after 8 min of UV irradiation, (d) zoom-in image. (e) Cross section along the white line in (a) showing that **P1** polymers exhibit a homogeneous height of 7 ± 1 Å. (f) Cross sections along the parallel blue and red lines in (b) and green dashed line in (d) showing a lamellar structure (width 6 ± 0.2 nm, lamellar peaks are indicated by vertical lines); the height of one rigid-rod polymer **P1,** centered at a "valley" of the ODA lamellae changes from *ca*. 0.7 nm to *ca*. 0.9 nm upon UV irradiation. The black line indicating a length of 9.8 nm defines the apparent width of the polymer, as estimated from a model sketched in (g).

Interestingly, deposited **P1** polymers exhibit a rather homogeneous height of h = 0.7 ± 0.1 nm, as indicated by a cross section profile (Figure 4.7e, along the white line Figure 4.7a). The experimental height approximately matches the expected molecular width of the backbone of **P1**, as estimated by the distance between two methyl groups placed in *meta*-position on one phenyl ring, $d_{methyl\text{-}methyl} \sim 0.5$ nm. The first two rods (numbered 1 and 2 in Figure 4.7e) have a characteristic width of 10 nm, which is defined as the thinnest apparent width among **P1** rods, and the distance between them is *ca*. 18 nm (about three lamellae). Note that the measured widths are broadened due to the finite SFM tip radius[78] (see discussion below for more details). The third and fourth rods (3 and 4) are separated by only 12 nm (about two lamellae), where the tip of the cantilever cannot go down to the surface due to the finite radius of the SFM tip apex, explaining why these two peaks are only partially resolved. The fifth polymer has a kinked spot, resulting in a slightly larger width. Although many closely aligned parallel polymers cannot be fully resolved by the SFM tip, some completely isolated rods can be identified.

Both **P1** polymers and ODA lamellar structures can be clearly seen in zoomed-in images (see Figure 4.7b). The blue line shows that the cross section of the lamellae (blue line in Figure 4.7f) exhibits periodic peaks and valleys (peaks are marked by vertical lines in Figure 4.7f) with the characteristic lamellae width of 6 ± 0.2 nm, which is very similar to the width prior to the deposition of **P1** (see Figure 4.11), indicating that the ODA monolayer was not altered by the deposition of the polymers. The red line in Figure 4.7b shows the cross section of a single **P1** polymer located above a valley of the lamella (see also red line in Figure 4.7f) with a width of *ca.* 10 nm.

The sample was irradiated with UV light ($\lambda = 365$ nm) for 8 min, (Figure 4.7 c). The color saturation (white) was set to 1.5 nm. One can observe that before irradiation nearly all **P1** polymers are under 1.5 nm height whereas after irradiation, several parts of **P1** polymers exceed 1.5 nm height. Besides the increase of the height, most of the rods were also shortened. Zoom-in images in Figures 4.7b and d highlight a polymer chain, which was shortened after irradiation and concomitantly exhibits an increase in height from 0.7 nm to 0.9 nm (see green dash line in Figure 4.7f)). The increase in height accompanied by the shortening of the rods indicates a shrinking process, which can be attributed to the *trans* $\rightarrow$ *cis* photoisomerization of the embedded azobenzenes. In order to evaluate the efficiency of this process, the level of contraction was measured on a large scale image as the change in the area occupied by the polymers, which amounts to a 23% decrease (see Appendix II, Figure A3).

Due to the finite radius of the SFM tip apex, lateral dimensions of objects are generally overestimated, since the tip starts to interact with the imaged object before the tip apex encounters it. In order to know if the measured characteristic width could

be the actual width of single polymer, the process of deconvolution was applied by using the following model (Figure 4.7g). I assume the cross section of a single **P1** polymer to be rectangular with a width *w* and height *h*. By assuming further that the tip is capped with a semisphere with radius *R*, the apparent width of a **P1** polymer can be estimated to be $L = w + 2\sqrt{2Rh - h^2}$. Here, I took *h* from the apparent height, $h = 0.7$ nm, and assumed the real width to be $w = 3.3$ nm (assuming that dodecyl chains of **P1** are fully stretched, possibly on the alkyl chains of the ODA molecules). Taking $R = 8$ nm, *i.e.* a typical tip radius, I obtained an apparent width of a single **P1** polymer to be $L = 9.8$ nm (black line in Figure 4.7f), which correlates well with the measured apparent width. Therefore, I attribute the **P1** rods with its characteristic width to the width of single polymers. The formation of **P1** dimers and higher aggregates is in any case not likely due to the bulky, highly twisted tetra-methyl biphenyl linkers present in the backbone of the polymer. In summary, based on the width, the height, and the geometry of the polymers, I can conclude that the measured rods are single (macro)molecules. This conclusion was further verified by the behavior of **P1** upon irradiation.

4.2.2.2 Light-induced contraction

In a further study, another sample was irradiated at λ = 365 nm for 30 s, 2 min, 4 min, 9 min, 19 min, and then at λ = 436 nm for 10 min to induce the *trans* → *cis* and back *cis* → *trans* isomerization, respectively (see Movie S1 for snapshots of **P1** polymers undergoing contractions and extensions). The width of the ODA lamellae seems to be unchanged after switching the **P1** polymers (see Figure 4.11), indicating that the ODA lamellae were not affected by the photo-irradiation.

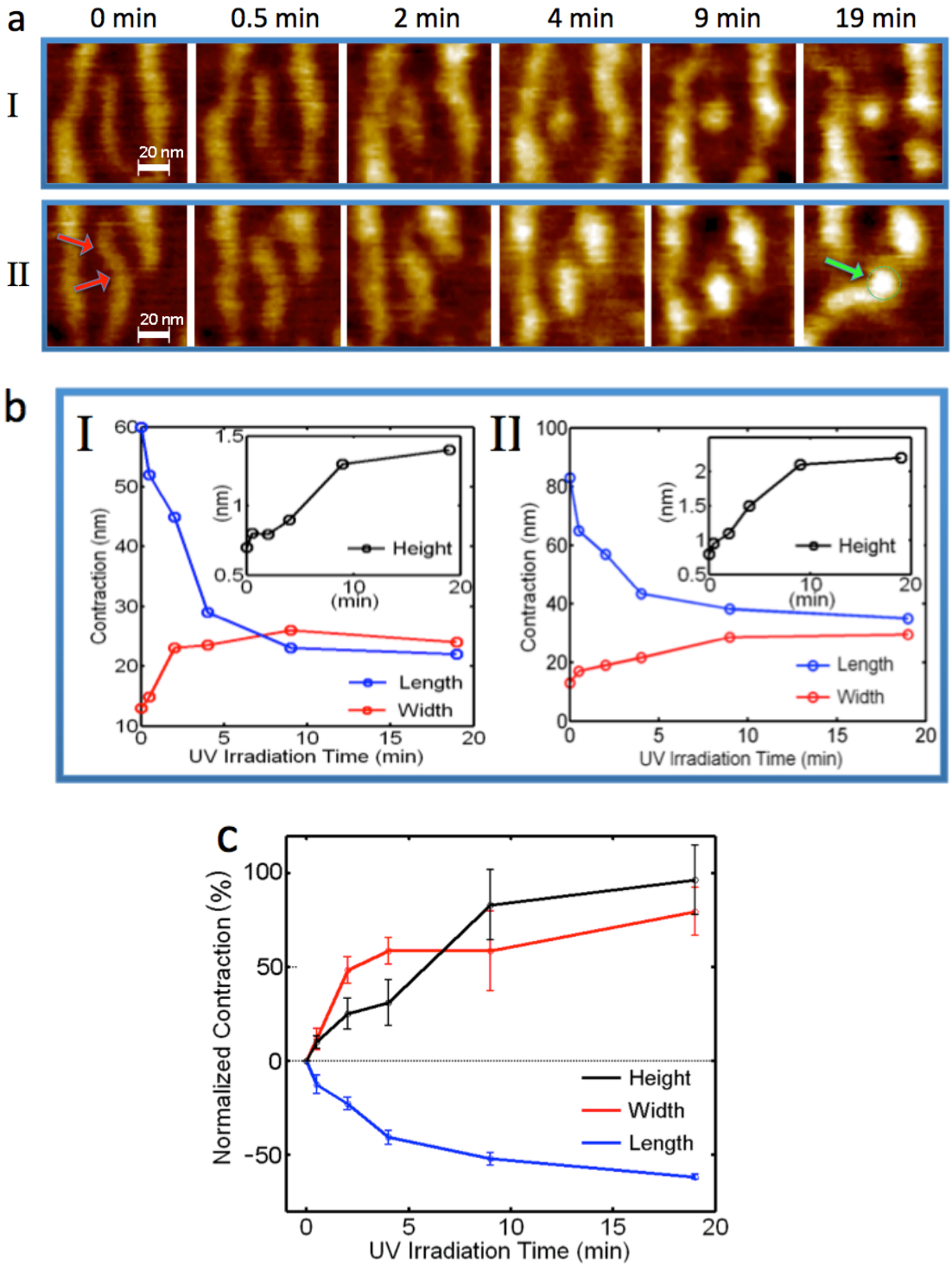

Figure 4.8 (a) SFM snapshots showing the shrinking of two single polymers (**I** and **II**) after UV irradiation for 30 s, 2 min, 4 min, 9 min, and 19 min (two kinks in single polymer **II** are indicated by red arrows). (b) Changes in length, width, and height (highest point) of the polymers **I** and **II** during irradiation. (c) Normalized contraction measured on six well-isolated single polymers with lengths ranging from 62 nm to 92 nm (mean values plotted with standard errors).

Figure 4.8a shows selected SFM zoom-in images of two different locations, following the contraction of two single rigid-rod **P1** polymers (**I** and **II**) upon UV-light irradiation. For **I** the apparent length changed from 60 nm (*ca*. 25 repeat units) to 22 nm (see Figure 4.8b, **I**), while the width increased from 13 nm to 24 nm and the height from 0.7 nm to 1.4 nm. After 19 min of irradiation, no further change in size was observed, indicating that the polymer reached a PSS. Both length and width attained nearly equal values, suggesting that the single chain has adopted a more compact, disk-like shape. Considering that the geometry of a single rigid-rod **P1** polymer is cylindrical, the aspect ratio can be defined as the ratio of the width to its length. Using the apparent widths and lengths, the aspect ratio was evaluated to change drastically, from 1/4.6 to 1/1, *i.e*. from a rod-like to a disk-like morphology. This particular change in aspect ratio was also observed in solution by light-scattering measurements.[25] Drastic contraction of ΔL = 38 nm (from 60 nm to 22 nm) was measured in that particular case, whereas for **II**, which is longer, this value reached ΔL= 48 nm (from 83 nm to 35 nm, see Figure 4.8b, **II**). Similar measurements performed on several other well isolated single polymers confirm this trend, *i.e*. upon UV-light irradiation lengths are typically reduced by about 60%, while heights and widths nearly double (see Figure 4.8c). The direct visualization of such high level of *directly* light-induced contraction in a single (macro)molecule is quite remarkable. It should be noted that another example of this kind, reported by Baigl and coworkers,[47] details the *indirect* light-fueled compaction of DNA, with azobenzene-containing polyamine aqueous solution acting as the photoswitchable medium, *i.e*. the motion of the DNA at the surface was induced by structural changes of surrounding molecules.

4.2.2.3 Nonlinear behavior of polymer's contracting process

Based on the observation of the nonlinear shrinking process in Figure 4.8b,c, one may try to elucidate the shrinking and extending process of these rod-like polymers on a surface. It is clearly seen that the shrinking of polymers (**I** and **II**) does not result in positional shift (though with only few exceptions, see following sections), indicating the shrinkages of the two sides from the center of the rod-like polymer are equal; therefore, the light's exposure on single polymer should be evenly distributed. Considering the light's exposure on a single polymer being uniform, the isomerization probability for azobenezenes at the backbone of the polymer should not be equal.

Due to the symmetric morphology of the rod-like **P1** polymer, the two sides of the polymer should have a symmetric distribution of isomerizing probability. If an azobenzene photoswitch at the center of the polymer is isomerized to perform the *trans* → *cis* transition, this would mean that in order to adopt the *cis* conformation the azobenzene should be able to move at least one long arm from either sides of the polymer, *i.e.*, exerting a higher force to overcome a greater steric hindrance, whereas the azobenzenes around the two ends of polymer only need to overcome the steric hindrance of the shorter part of the polymer. In other words, in the beginning of the irradiation the azobenzenes embedded around the two ends of a polymer should have a higher probability to be switched. Therefore, I assume the azobenzene photoswitches around two ends will be switched earlier. This assumption coincides with the observation of nonlinear behavior in Figure 4.8.

In the early stage of UV irradiation (corresponding to the first five minutes of polymer **I** in Figure 4.8), some azobenzene photoswitches around the two ends of polymer are the first to be contracted, resulting in rapid shrinkage of the polymer (about 30 nm). During this early stage, however, the increase of the height of the

polymer (only by 0.3 nm) was not as noticeable, indicating that the conformational change of azobenezene in this stage mainly causes shrinkage in length. The small increase in height may indicate that isomerization of azobenezenes in this stage does not need to move the longer part (arm) of the polymer.

In the next stage of UV irradiation (corresponding to 10 minutes time of UV irradiation), the shrinkage of length and broadening of width are approaching saturation, yet the height increases noticeably to two times of its original height (polymer **I**) or three times (polymer **II**). In this stage, azobenezenes (probably closer to the center of polymers) could isomerize by moving larger parts of the polymer that translated to an increased height and a broadened width.

In the final saturating stage of UV irradiation (corresponding to 19 minutes of UV irradiation), changes in all three dimensions of polymer have reached saturation in photostationary state (PSS).

4.2.3 Crawling movement of polymer on surface

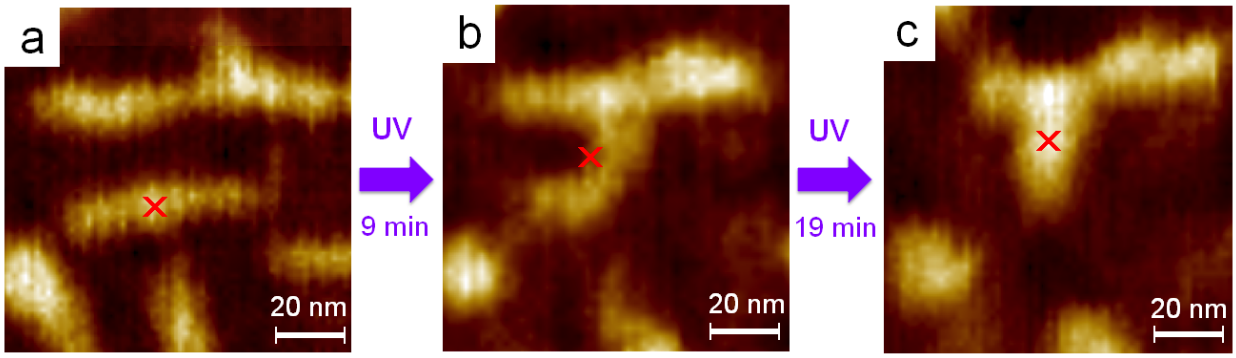

Figure 4.9 SFM snapshots of the same location (extracted from Movie S1, green frame) showing the crawling movement of a single **P1** polymer upon UV-light irradiation for 9 min and 19 min. The bending (b) and shrinking (c) of the polymer results in a translational movement, indicated by a *ca*. 10 nm shift of the center of the macromolecule (see red cross).

Besides the light-induced formation of disk-shaped single-chain polymeric nanostructures associated with the high levels of contraction, I also observed crawling movements of some polymers during UV-light irradiation. Figure 4.9 shows SFM snapshots of the same location (extracted from Movie S1, green frame), where a polymer, which was initially fully stretched (Figure 4.9a), is contracted and at the same time, shifts its center over *ca*. 10 nm (see the red cross). In the snapshot it is evident that this translation was achieved through subsequent bending and contraction of the backbone, resembling a crawling motion. This particular movement is an additional strong proof that the observed polymer is indeed a single macromolecule.

The crawling movements of azobenzene-polymers on surface could be seen as a consequence of photo-isomerization. Especially, the directional bending of a single polymer suggests anisotropic interactions that are present during irradiation. I assume that this anisotropic interaction should have come from the microenvironment, namely, the underlying molecular surface, surface defects or neighboring polymers. As it is a common observation that aggregation takes place during photo-isomerization, I assume the directional bending to be due to intermolecular interaction between polymers while the photo-isomerization is taking place. The crawling movements enable one single **P1** polymer to move toward (or aggregate) to another polymer (see Figure 4.9). As the light is generating more *cis* isomers and thereby dipole moments, the dipole-dipole interaction within and between polymers may become the source of anisotropic interaction in their local environment. **P1** polymers (in Figure 4.9) are in close distance (≈10 nm) to its neighboring polymers, a distance that allows polymers to interact while letting SFM to track its bending. More

discussions about the influence of the local environments on **P1** polymers will be in chapter 4.3.

4.2.4 Light-induced extension

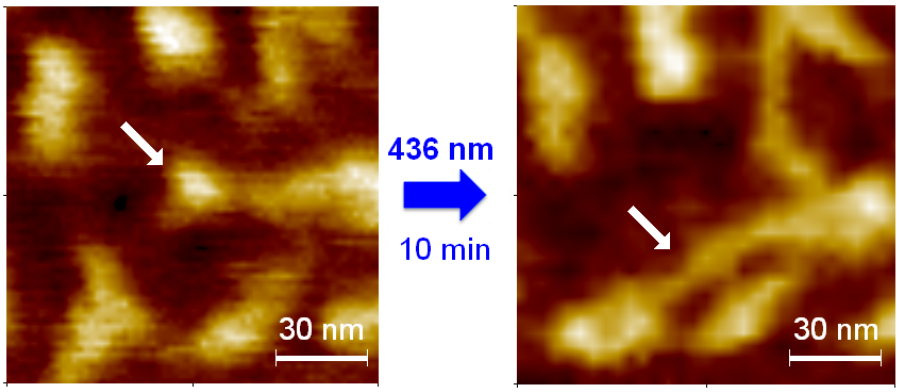

Figure 4.10 SFM images of the same location (extracted from Movie S1, red frame) showing a **P1** disk-like polymer nanostructure that extends (see arrows) upon irradiation at λ = 436 nm for 10 min, as a result of the *cis* → *trans* isomerization of the azobenzenes in the backbone.

Following UV-light irradiation, I irradiated the same sample with visible (λ = 436 nm) light in order to investigate the reversibility of the process, *i.e.* to induce the stretching of the previously contracted polymers. In a selected SFM image (Figure 4.10), one globular structure extends dramatically (see arrows, extended distance ≈ 30 nm), as a result of the *cis* → *trans* isomerization of the azobenzenes. Several of these newly extended rod-like structures can be found after blue-light irradiation, but not all of the polymers were stretched back. Clearly, azobenzenes in *cis*-rich **P1** are not as photoactive as they are in the rod-like geometry of *trans*-rich **P1**, possibly due to an increased steric hindrance and lack of free volume inside the polymeric particle.

4.2.5 Preservation of ODA lamellae after irradiation

It has been reported previously that ordered/disordered amphiphilic monolayers of dodecylamine on HOPG can affect the morphologies of on-top deposited macromolecules.[99] In that report raising the temperature could cause the transition of the dodecylamine monolayer on HOPG from an ordered to a disordered structure such that the width of the dodecylamine lamellae becomes larger and eventually disappeared in the SFM image.

In order to determine the influence of temperature on both the ODA monolayer and **P1**, the sample was heated up to 55°C (the ODA's melting point is 52 °C). The results (see Appendix III) show that the rod-like morphology of **P1** was unchanged even at 45°C and the changes were found only after heating above the melting point of ODA. This indicates that the ODA monolayer is relatively insensitive to temperature, which may be attributed to ODA's longer alkyl chains that formed a more stable lamellar structure on HOPG.

Furthermore, in order to determine if the observed conformational changes of **P1** polymers are influenced by the changes in the underlying molecular substrate, here, I checked the morphological integrity of ODA lamellae on HOPG before (Figure 4.11a) and after deposition of **P1** polymers (Figure 4.11b), after UV irradiation (Figure 4.11c) and after blue light irradiation (Figure 4.11d).

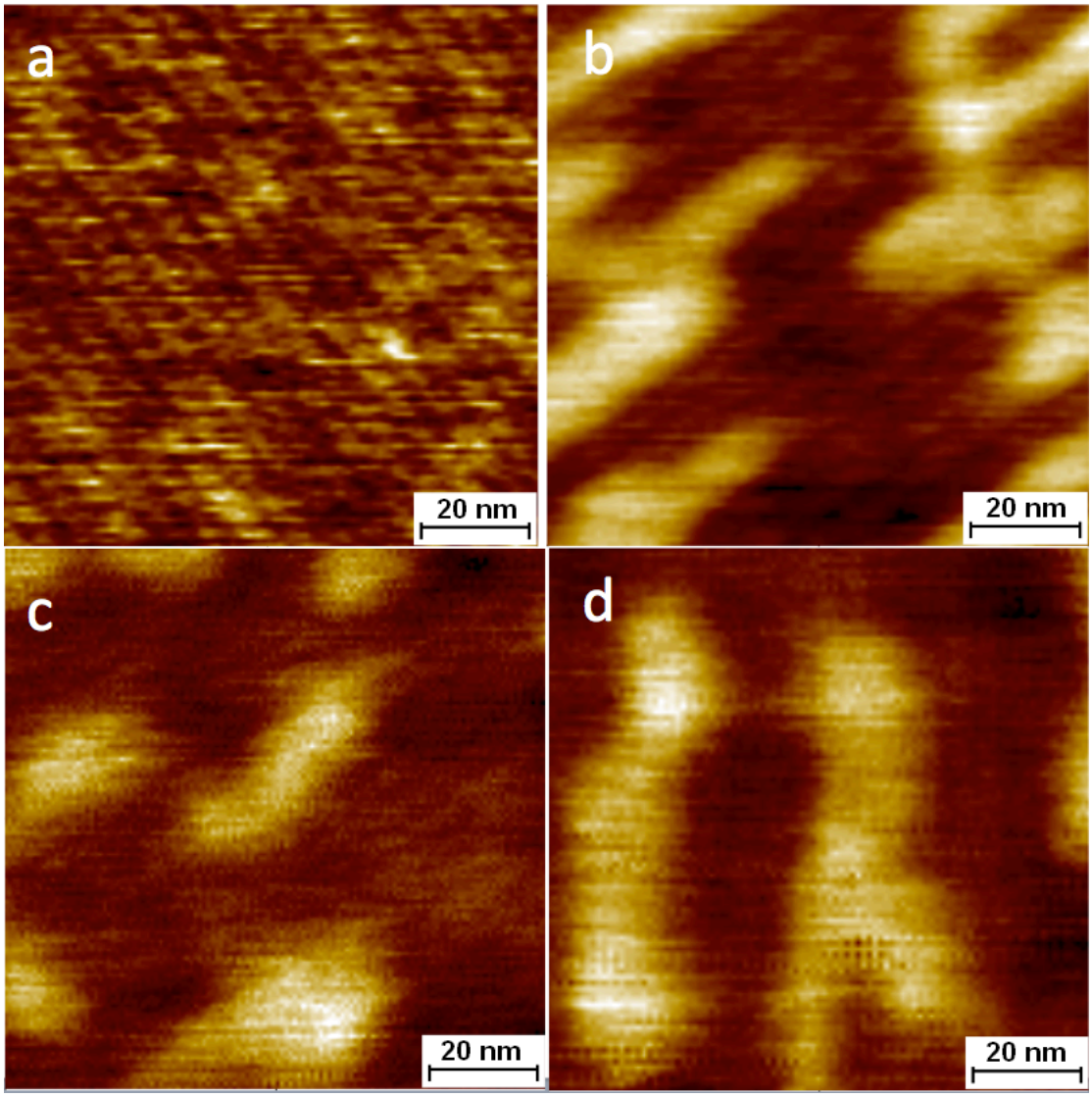

Figure 4.11 (a) In the zoomed-in SFM image (100nm×100nm), the ODA lamellar structure was formed on graphite with a width w = 6 ± 0.2 nm, measured by the Fourier transform of the image. (b)After deposition of **P1** polymer, the ODA lamellae were preserved with a width of w = 6.3 ± 0.3 nm. (c) After 19 minutes of UV irradiation, the lamellae remained observable with a width w = 5.8 ± 0.3 nm. (d) Finally, after 10 minutes of 436 nm irradiation, the lamellae remained observable with a width w = 5.7 ± 0.3 nm. The morphology of the lamellar structure remained straight and undistorted even in the regions close to **P1** polymers.

The results in Figure 4.11 showed that the morphology as well as the width of the ODA lamellae were not substantially altered by the deposition of **P1** polymer or irradiation with light of different wavelengths (the variations lie within the error of the

measurement). Therefore I assume that the ODA lamellae remain orderly adsorbed on the graphite surface.

4.2.6 Conclusion

In conclusion, I demonstrated that single rigid rod-like azobenzene-containing macromolecules can be immobilized, oriented and isolated on the well-defined surface of a self-assembled ODA monolayer tiling HOPG. Dramatic contractions and extensions of single macromolecules on the surface were induced by light irradiations with different wavelengths. The successful photoisomerization processes can be attributed to the weak mechanical and electronic coupling of the polymer with the surface due to the isolating molecular monolayer. This study reports the *directly* light-induced motion of single macromolecules at a surface, which is visualized and analyzed in detail. Besides the internal motion of the polymers, light-induced crawling movements of single polymers on a surface were described. Further control over the directionality should be possible—for example through the use of polarized light and more mobile templates—in order to develop useful optomechanical nanomachines.

4.3 Directed intramolecular motions of single zobenzene-containing polymers on heterogeneous ODA surface induced by light

4.3.1 Introduction

In the previous sections, the synthetic rigid-rod polymers (**P1**) incorporating multiple azobenzene photoswitches were oriented on octadecylamine-modified surface and the light-induced movements were visualized by *in-situ* scanning force microscopy. In this section 4.3, I will discuss the role of the ODA molecular substrate in orienting or directing the contracting/extending movements of the polymers on the surface.

Controlling the molecular motion along a one-dimensional track on a surface is a fundamental challenge in the field of molecular machines.[87] Inspired by natural motor proteins, such as kinesin-I,[100,101] that can move along a one-dimensional track of polymeric filaments, scientists have employed molecular "tracks" that restrict the degrees of freedom of moving molecules powered by external stimuli; for example, a molecular "spider", fueled chemically, can be guided along a DNA origami track,[84] or pulling mechanically a pinion-like molecule along the edge (track) of a self-assembled molecular island causes the directional rotation of that molecule.[5]

Self-assembled molecular monolayers, sometimes acting as templates for the adsorbates, provide complex landscapes that can be potentially utilized as molecular tracks. As being demonstrated in 4.1, octadecylamine (ODA) self-assembled on a graphite surface provides amphiphilic lamellae (nano-rails) that orient the deposited **P1** polymers to either parallel or perpendicular orientation (with respect to lamellar

axis). Beside the landscape of lamellae, self-assembled ODA monolayer on graphite also provides the landscape of one-dimensional domain boundaries and edges of surface defects (see Figure 4.13a). Theses one-dimensional "lines" of lamellae or domain boundaries shown in scanning force microscopy reflect the asymmetrically arranged ODA molecules self-assembled on a graphite surface, which could be potentially utilized as "tracks" for directed molecular motion.

Here, I will focus on how the directions of intramolecular movements (contracting/extending) of **P1** polymers are correlated with the underlying heterogeneous ODA monolayer. The *in-situ* directional changes of contracting/extending movements of **P1** polymers will be compared from the SFM images after each irradiation wavelength, composing 3 irradiation cycles.

4.3.2 Switching probability of single P1 polymers on heterogeneous ODA surface

First of all, **P1** polymers in solution of low concentration (0.005 g/L) were spin coated onto an ODA monolayer tiling the graphite surface without any light pretreatment. The SFM image in Figure 4.12 shows the typical **P1** rod-like polymers on top of a self-assembled ODA monolayer. The three main landscapes of the ODA surface, on which most of **P1** polymers were absorbed, are domain boundary (see Figure 4.13, Polymer I), lamellar structures (see Figure 4.13, Polymer II) and surface defects (see Figure 4.12, Polymer III).

Then, the three UV/Vis irradiation cycles were performed by illuminating with UV light for 19 minutes and blue light for 10 minutes. These are time spans, which have been demonstrated previously (see section 4.2) to be long enough to drive single **P1**

polymers to their *cis*-rich and *trans*-rich photo-stationary states. By comparing SFM images taken after each irradiation, the changes in size and morphology of the polymers were measured.

Here the statistics of the switching probability of single **P1** polymers on an ODA surface was done as followings.

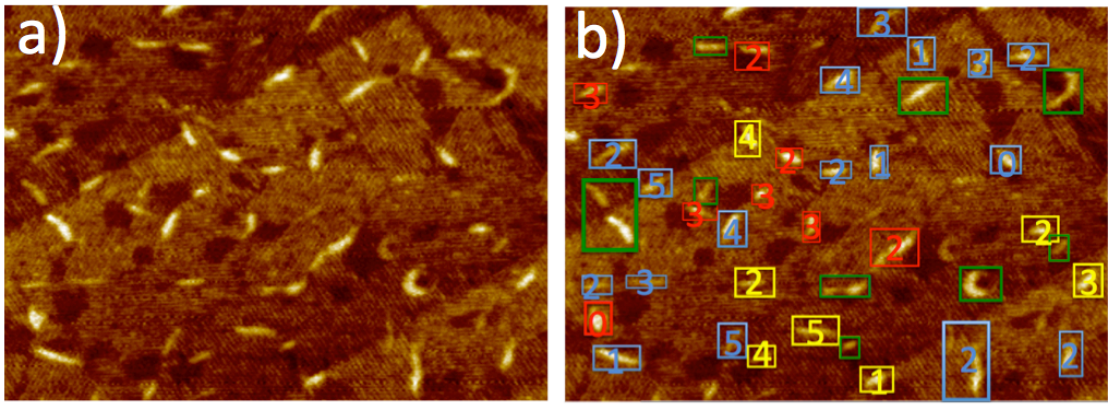

Figure 4.12 (a) The SFM topographic image showing **P1** rod-like polymers deposited and isolated on different landscapes of lamellae, domain boundary and edge of surface defect of ODA surface. (b) The polymers on ODA lamellae were marked in yellow; on domain boundaries were marked in blue; on the edge of ODA surface defects were marked red; The polymers with unclear (or mixed) local environment due to the quality of the image or polymeric bundles, or aggregation took place during irradiation, were marked green, which will not be taken into calculation.

First, the isolated **P1** single polymers on different landscapes of an ODA surface were identified, as shown in Figure 4.12 (a). I categorized these polymers according to their local environment from the three main landscapes of an ODA surface, namely, lamellar domain, domain boundary and surface defect. (Other landscapes, such as step edges of graphite or contaminations on the surface are not taken into account.) The polymers on the ODA lamellae were marked with yellow rectangles (see Figure 4.12 b), the polymers on the ODA domain boundaries were marked in

blue rectangles, and the polymers on the edges of ODA surface defects were marked in red rectangles. Polymers with unclear (or mixed) local environment, not easily (due to the quality of the image) identifiable, polymeric bundles, or with aggregation taking place during irradiation, were marked with green rectangles, which will not be taken into calculation.

The second step is to count the times of successful switching for every individual polymer for 3 UV/Vis cycles. I accumulated 7 SFM-images into a movie (see Movie S2) in order to see the changes during the irradiation cycles. Here, I considered a successful switching observed in SFM images if there is either a noticeable length change (10~30% contraction or extension depending on quality of image) or a noticeable morphological rod-coil transition. Ideally, if switching probability were 100%, every **P1** polymer would experience 6 times of a length change for three UV/Vis irradiation cycles. However, in reality, not every irradiation induces noticeable changes of the polymer's length or morphology in the SFM images. By comparing SFM images (three examples are in Figure 4.13), the number of successful switching of each polymer was counted (as being indicated by the numbers in Figure A5b). The results of this statistics (see Figure 4.12b) are shown in table 4.1, showing that the averaged switching probability of 32 single polymers to be 42 %.

Times of switching / Landscapes	0	1	2	3	4	5	Numbers of polymers	Averaged switching probability
Lamellae	0	1	2	1	2	1	7	50.0%
Domain boundary	1	3	6	3	2	2	17	41.2%
Surface defects	1	3	4	0	0	0	8	37.5%
						Total	32	42.2%

Table 4.1: The averaged switching probability of 32 single **P1** polymers in Figure A5 according to three different landscapes of ODA's lamellae, domain boundary and surface defect.

The relative low switching probability I observed here may be due to the limited capability of the SFM to detect small motions within the polymer. Some error in the length measurement is due to the finite tip's apex, which hampers exact length determination. Another error is due to non-identical conditions in the measuring cycles, which may come from different sources, such as slightly different alignment/focus of the irradiating light, leading to different energy input. The different time needed in searching the polymers on the surface and SFM image acquisition may lead to different degrees of polymer's relaxation at room temperature. The perturbation from the tapping of SFM tip during scanning could also affect the kinetics of the polymer's relaxation.

I also find that the changes in the polymer's length and morphology are not fully identical in each irradiating cycle (see more clearly in figure 4.13). It may be due to different folding (contracting) or unfolding (extending) routes of the polymers. From the polymer's point of view, unlike small molecules that switched between simply two states, light-induced movement of a macromolecule like **P1** polymer is the collective motion of many mutually affecting/coupling motions of azobenzenes and therefore, more complicated. For example, polymer (I) in figure 4.13 with the length of 47 nm corresponds to 38 azobenzenes in the main chain. Therefore, if different azobenzene monomer in the backbone of the polymer switched at different times, it may lead to different folding/unfolding routes, resulting in different final size and shape. The heterogeneous ODA monolayer also adds the difficulty to understand the detailed folding/unfolding process of the polymer.

4.3.3 Directed intramolecular motions of P1 polymers on a heterogeneous ODA surface

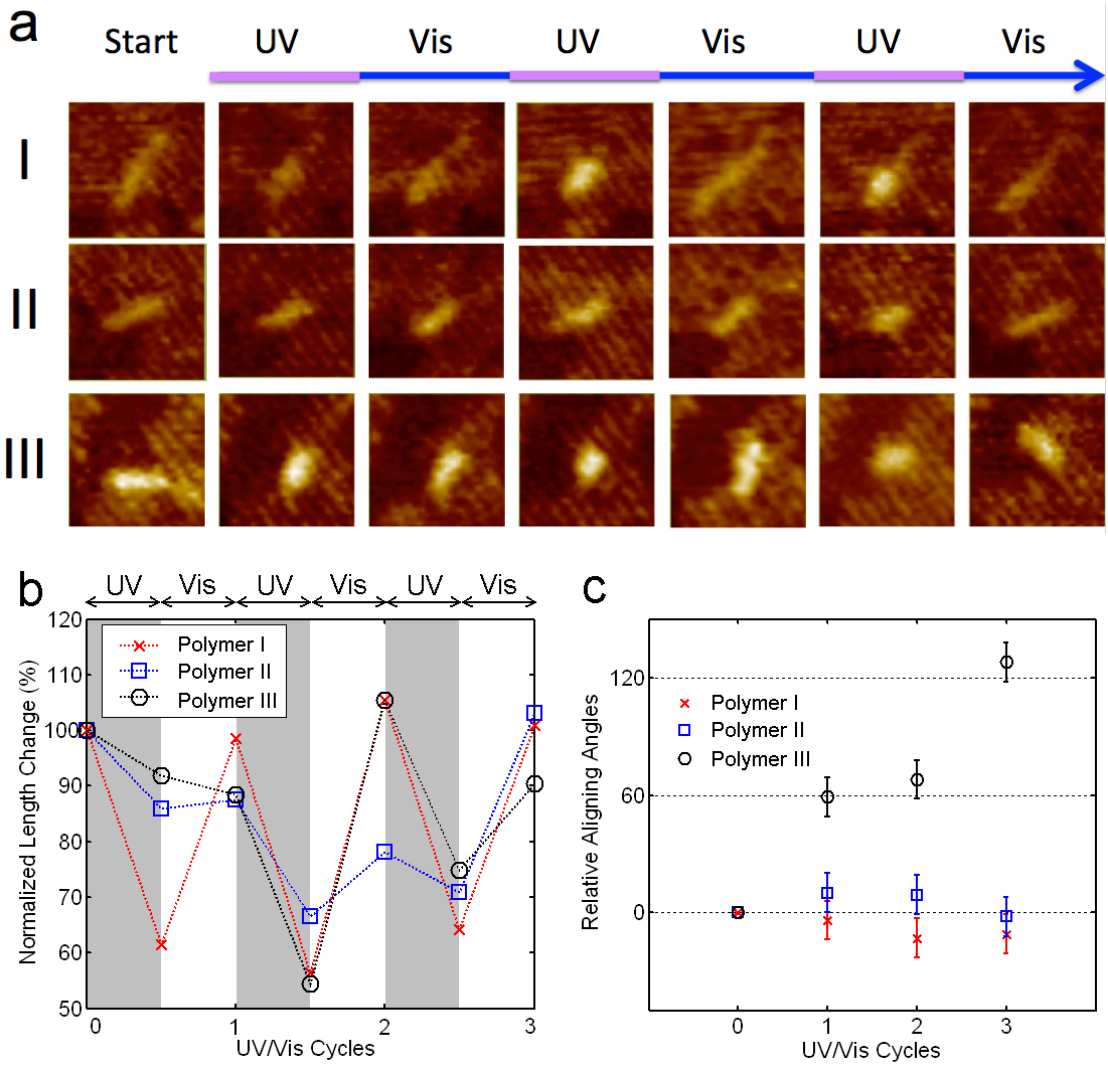

Figure 4.13 (a) SFM images of three selected **P1** polymers representing three ODA landscapes measured during three UV/Vis irradiation cycles. Polymer I was on a domain boundary. Polymer II was lying perpendicular to the ODA lamellae. Polymer III was at one edge of a surface defect. (b) The length changes of the three polymers during the 3 UV/Vis cycles. (c) The relative aligning angle of the three polymers during 3 UV/Vis cycles.

Figure 4.13 shows the SFM images of three **P1** polymers numbered I, II, III, representing different landscapes of ODA, on which polymers are absorbed. Polymer

(I) is lying on a linear domain boundary of ODA surface, polymer (II) is lying perpendicularly to the ODA lamellae, and polymer (III) is lying along a boundary between a lamellar domain and a surface defect (indicated by a dark area).

After the deposition of **P1** polymers on the ODA lamellae (shown in "start" column), i.e., before the irradiation, the **P1** polymers exhibited a rather extended rod-like morphology, indicting the *trans*-rich state.

Polymer (I) underwent movements of contractions and extensions as the length changed during 3 UV/Vis cycles (Figure 4.13b). Although Polymer (I) was one of the few polymers considered with 5 times successful switching (see table 4.1), it demonstrated the possibility of a single **P1** polymer to perform repetitive contracting/extending motions. As shown in figure 4.13b, the changes of the polymer's apparent length in each cycle are not fully identical. Moreover, the shapes of the polymer (I) after each irradiation are not fully identical. The main trend of this result, however, is in accordance with the result in section 4.2, where the **P1** polymer contracted by irradiating UV light and extended by irradiating blue light (though due to aggregation only one cycle was demonstrated).

It is also shown that in each step of irradiation, polymer (I) contracted and extended along the domain boundary. Measuring the orientations of extended polymer (I) after three times of irradiation with blue light (for the extended form of the **P1** polymer it is easier to measure the angles), the relative aligning angles (the aligning angle changed related to polymer at "start") stay close to zero (see Figure 4.13c), indicating the molecular extension motion was "sticking" to the linear track of this domain boundary. This indicates in a microscopic view that the motion of extension (*cis*→*trans*) of azobenzene unites in the backbone of the polymer is somehow

modified and directed by the underlying ODA domain boundary. While one may expect that the contracting motion of polymer **P1** should pull the two ends of the polymer towards its center, it is not trivial that the stretching movement of the polymer would be also directionally fixed in one direction.

Polymer (II) on a lamellar domain experienced similar contractions and extensions during irradiating cycles. It exhibits rather small changes due to its shorter length. It is also noticeable in figure 4.13 (b) that the length changes of polymer (II) are not the same in each cycle as well as the shapes are identical, which is similar to polymer (I).

Lying in the start perpendicularly to the lamellae of ODA, polymer (II) stayed in the same direction throughout the 3 irradiation cycles, as indicated by relative aligning angles around zero in Figure 4.13c.

Polymer (III) underwent also contractions and extensions according to the irradiation (see normalized length change in Figure 4.13b). Lying on an edge of a surface defect (dark area in Figure 4.13a), polymer (III) changed its orientation stepwise as indicated by the changes of its relative aligning angle (in Figure 4.13c). Polymer (III) rotates firstly counterclockwise 60° after two irradiating cycles and rotates further 60° after a third irradiating cycle, adding up to totally 120° of rotation. The rotation clockwise or counterclockwise is dependent on the coupling of the actuating polymer with the delicate edges of the surface defect. Nevertheless, the difference of 60° each time reminds of the 3-fold symmetric alignment of ODA molecules on graphite. It is clearly seen that polymer (III) changed its orientation form one edge of the surface defect to another. Such orientation changes took place not continuously but stepwise by alternating lights of different wavelengths.

The change of the polymer's alignment could be further elucidated in the following example where a polymer strand was partially on the lamellae and partially on a domain boundary.

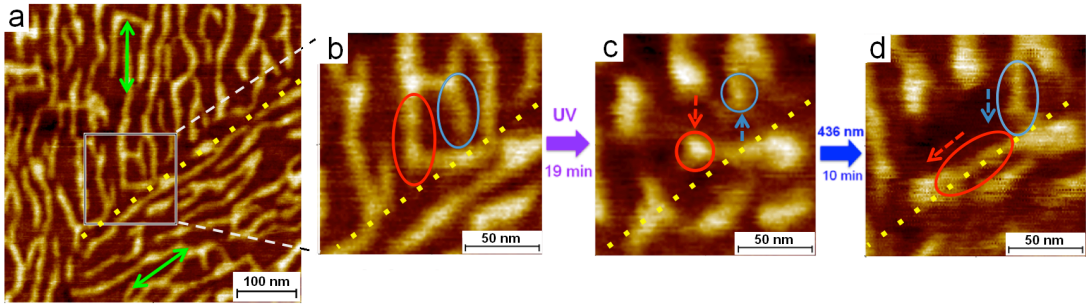

Figure 4.14 (a) SFM image of **P1** polymers on an ODA monolayer with a domain boundary (marked by yellow dotted line). The two green arrow lines denote the directions of the ODA lamellae within each domain. (b) The zoom-in image shows the upper part of a polymer (marked by red ellipsoid) that was in the lamellar domain while the other part of the polymer was on a domain boundary. Another polymer strand marked by blue ellipsoid was fully on the lamellar domain (c) After 19 minutes of UV irradiation, both polymers contracted to a globular shape as marked by red and blue circles. The arrows indicated the direction of the contracting movement. (d) After 10 minutes of 436 nm irradiation, both polymer strands stretched back to the rod-like shape (marked by red and blue ellipsoids). The arrows indicated the direction of their stretching movement.

Figure 4.14a shows a SFM image of **P1** polymers (deposited from solution of higher concentration, 1 g/L) on an ODA surface with landscapes of two ODA lamellar domains in two different directions (indicated by green arrows), and a domain boundary (marked by a yellow dotted line). The two green arrow lines with an angle difference of 60° reflect the 3-fold symmetry of the ODA lamellae on the graphite surface. The zoom-in image (b) shows a kinked polymer whose upper part (marked by a red ellipsoid) was on the lamellar domain while the other part was on the domain boundary. One neighboring polymer strand was completely on an ODA lamellar domain (marked by a blue ellipsoid). After 19 minutes of UV irradiation,

both polymer strands contracted as marked by red and blue circles in (c). The arrows indicated the directions of the polymers' motions, which are parallel to the lamellar axis as expected. I suppose that the contractions of both polymer strands stay within the hydrophobic "rails" of the ODA in order to avoid the unfavorable contact with the hydrophilic rails of ODA (see Chapter 4.1).

After 10 minutes blue light irradiation, both polymers stretched to a more extended form as marked by red and blue ellipsoids in (d). While the stretching direction (indicated by blue arrow) of one polymer went along with lamellar axis, the other polymer, interestingly, stretched in the other direction along the domain boundary (indicated by red arrow). The relative alignment angle after one UV/Vis cycle changed counterclockwise for about 120°, a number which again reflects the 3-fold symmetry of the underlying ODA surface.

It is most likely that the contracted form (marked by red circle in figure 4.14c) was already in the vicinity of the domain boundary, or, in more physical terms, already in a local energy minimum of the surface potential landscape of the domain boundary. The "turn" of the polymer may most likely happen with the polymer in the contracted form due to its weaker association with the surface. I do not rule out the possibility that the disturbance from the scanning tip of SFM may also rotate the polymer of lightweight.

The stretching motion (*cis*→*trans* isomerization) of the **P1** polymers along one direction can be explained by the simple argument that due to azobenzene's covalent bonds in the linear backbone of the polymer, the "backward" stretching is forbidden and forward stretching would encounter less steric hindrance. In other words, there is an asymmetric potential energy landscape along the backbone of the polymer, which determines the direction of azobenzenes' *cis*→*trans* movement. Such asymmetric

potential energy landscape is one of the fundamental requirements for the directional molecular motion to occur.[4]

Despite of all of these complicated molecular motions coupled with surface, the relative aligning angle change of 60° or 120° and the directional motion (especially the stretching motion) on ODA domain boundaries, lamellae and the edges of surface defect, reflected clearly the nature of the heterogeneous ODA surface and its function in directing the intramolecular motion of the **P1** polymer.

4.3.4 Conclusion

In conclusion, I demonstrated the oriented contracting/extending movements of unbound single **P1** polymers on a heterogeneous ODA surface. The well-defined local environment, such as a domain boundary or the lamellar structure of the ODA surface, plays the role of a "track" in directing the intramolecular motions of **P1** polymers during the photo-isomerization. In some cases an alternating irradiation with light could change stepwise the polymer's orientation and position, the directionality of which may be further controlled—for example through the use of polarized light and carefully-designed templates—in order to develop useful optomechanical nanomachines.

Chapter 5

Summary and Outlook

In summary, I demonstrated that single rigid rod-like azobenzene-containing macromolecules (**P1**) can be immobilized, isolated and oriented on the well-defined surface of a self-assembled ODA monolayer tiling HOPG. The surprising perpendicular alignment of **P1** along with a parallel alignment with respect to the underlying lamellar surface is found at relatively low surface coverage. Both parallel and perpendicular alignments can be qualitatively explained by a model based on the hydrophobic interaction of the side chains of the polymers with the amphiphilic nanorails, which may help for future theoretical modeling of molecular alignments on the surface and also the design of a bottom-up fabrication of molecular systems.

Single rod-like azo-polymers, undergoing contraction and extension movements by irradiations at different wavelengths, were directly visualized on the surface. Exposing a *trans*-azobenzene polymer to UV light was observed to gradually decrease its aspect ratio from a rod-like morphology to a disk-like morphology. Especially, the dramatic decrease in the polymer's length suggests a high efficiency of transducing photons into large mechanical movement. This successful photoisomerization is attributed to the weak mechanical and electronic coupling between polymer and surface, due to the isolating monolayer as well as the high density of azobenzenes in the polymer backbone. In the future this may be utilized for large-amplitude motions of **P1** polymers to perform useful tasks, such as to move or manipulate other molecules.

Besides the internal motion of the polymers, a light-induced crawling movement of single polymers on the surface was described. The crawling movement can be seen as a consequence of light-induced movements and was attributed to intermolecular interactions with neighboring polymers.

The influence of the local environments on the light-induced molecular movements was further investigated by probing the repetitive switching of single polymers on different sites of the heterogeneous ODA surface. I demonstrated the surface-oriented folding/unfolding (or contracting/extending) movements of unbound single polymers on a heterogeneous ODA surface that can be repetitively induced by light. The well-defined local environment, such as a domain boundary or a lamellar structure of the ODA surface, plays an important role in directing the folding and unfolding movements of azo-polymers during photo-isomerization. In the case of weakly adsorbed azo-polymers on an ODA surface defect, alternating irradiation of light at different wavelengths could change stepwise the polymer's orientation and position. Another step of pursuit could be to rotate and move the macromolecule in a controlled way—for example, by the use of polarized light and more mobile templates—in order to develop useful optomechanical nanomachines.

In general, the possibility to isolate single molecular machines from solution while maintaining their stimuli-excited responses is a crucial step towards any device application involving self-assembled nanostructures. The ability of isolating unbound single azo-polymers on a surface opens up the exciting possibility to directly visualize light-induced movements at the single-molecular level and to test fundamental molecular photoisomerization theory as well as the consequences it entails. Further studies on the detailed movements of single polymers should involve the development of a model including all the species involved in the photochemistry and the

optomechanical dynamics. In any case, muscle-like **P1** polymers have exhibited large light-induced conformational changes both in solution and on a surface and can be used as a key building block for the further development of nanomachines or incorporating them into various architectures for the access of macroscopic responses.

Appendix I:

Mathematical formulae for modeling the alignments of P1

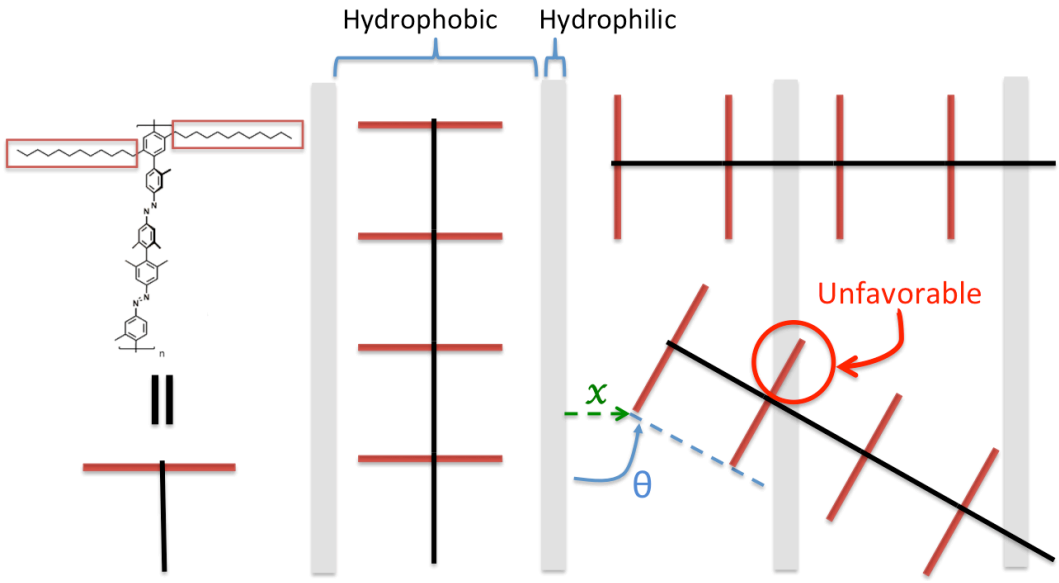

Figure A1 A polymer rod is represented by a straight black line (representing the backbone) and a red line orthogonal to it (representing a pair of dodecyl side chains) that prefer to align parallel or perpendicular to the amphiphilic "nano rows" of octadecylamine.

The variables are defined as follow:

L: representing the width of a hydrophobic row (4.64 nm) of ODA on graphite

l: representing the width of a hydrophilic row (0.53 nm) of ODA on graphite

A: representing the width of stretched dodecyl side chains

a: representing the length of a monomer

n: representing the degree of polymerization

i : representing the *i* th monomer in a polymer rod. The polymer is composed of monomers from *i*=1,2, …n

j : representing the *j* th hydrophilic row. *j* = 1,2,…

θ : aligning angle, representing the angle between polymer's backbone and a hydrophilic row

x : translational displacement, representing the distance from a hydrophilic row to the left end of the polymer's first side chain, as sketched

y_i : unfavorable contact length of i th monomer's side chain on hydrophilic row.

Y : the total length of unfavorable contact, $Y=\sum_{i=1}^{n} y_i$

Now I define the starting point when the polymer strand is on a hydrophobic row, aligned parallel to lamella of ODA (aligning angle $\theta = 0°$), with left side of polymers' side chains touching ($x = 0$). Taking the left end of the polymer's fist side chain as the turning axis (fixed point), the polymer strand starts to rotate anticlockwise (θ is increasing) until $\theta = 90°$, which is sufficient to reflect the behavior of the polymer from $\theta = 90°$ to 180° due to the symmetrical geometry of the lamellae.

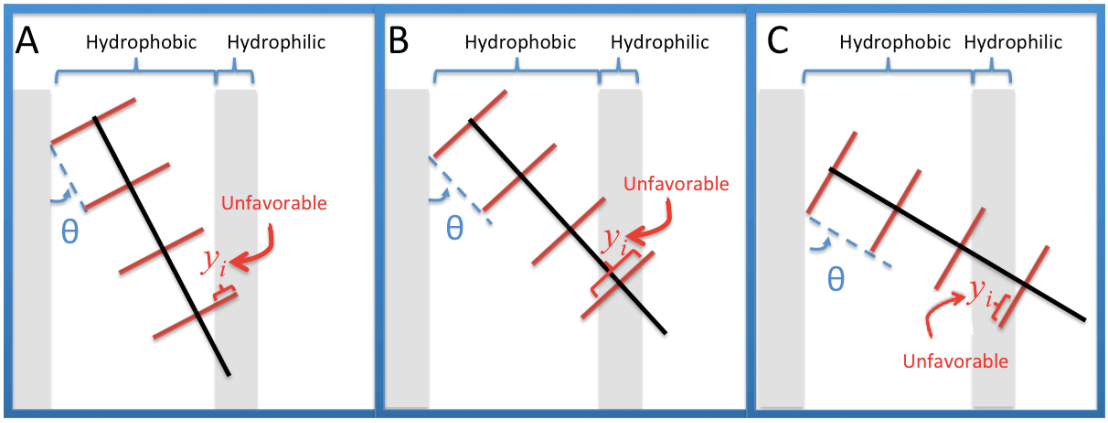

Figure A2 Schematics of three situations on a given dodecyl side chain (i) contacting its underlying hydrophilic row while increasing the aligning angle (θ). A) Only the right end of dodecyl side chain on top of the hydrophilic row. B) Two ends of the dodecyl side chain are not on top of the hydrophilic row. C) Only the left end of dodecyl side chain on top of the hydrophilic row.

As the aligning angle of the polymer is increasing, any given side chain i could undergo the following three situations, as illustrated in Figure A2. Firstly, a part of the polymer's side chain i (counting from the right) on top of the hydrophilic row is illustrated in (A). That is,

when $j(L+l) > ia\sin\theta + A\cos\theta > j(L+l) - l$

$$y_i = A - \frac{j(L+l) - l - ia\sin\theta}{\cos\theta}$$

As the aligning angle increases further, the side chain i could be covering the hydrophilic row, leaving some parts from the two ends on the hydrophobic row, as illustrated in (B). That is ,

when $ia\sin\theta + A\cos\theta > j(L+l)$ and $ia\sin\theta < j(L+l) - l$

$$y_i = \frac{l}{\cos\theta}$$

Finally, before side chain i leaves ths hydrophilic row, a part of the polymer's side chain i (counting from the left) will be on top of this hydrophilic row, as illustrated in (C). That is,

when $j(L+l) > ia\sin\theta > j(L+l) - l$

$$y_i = \frac{j(L+l) - ia\sin\theta}{\cos\theta}$$

Appendix II: Shrinkage of P1 polymers upon UV irradiation

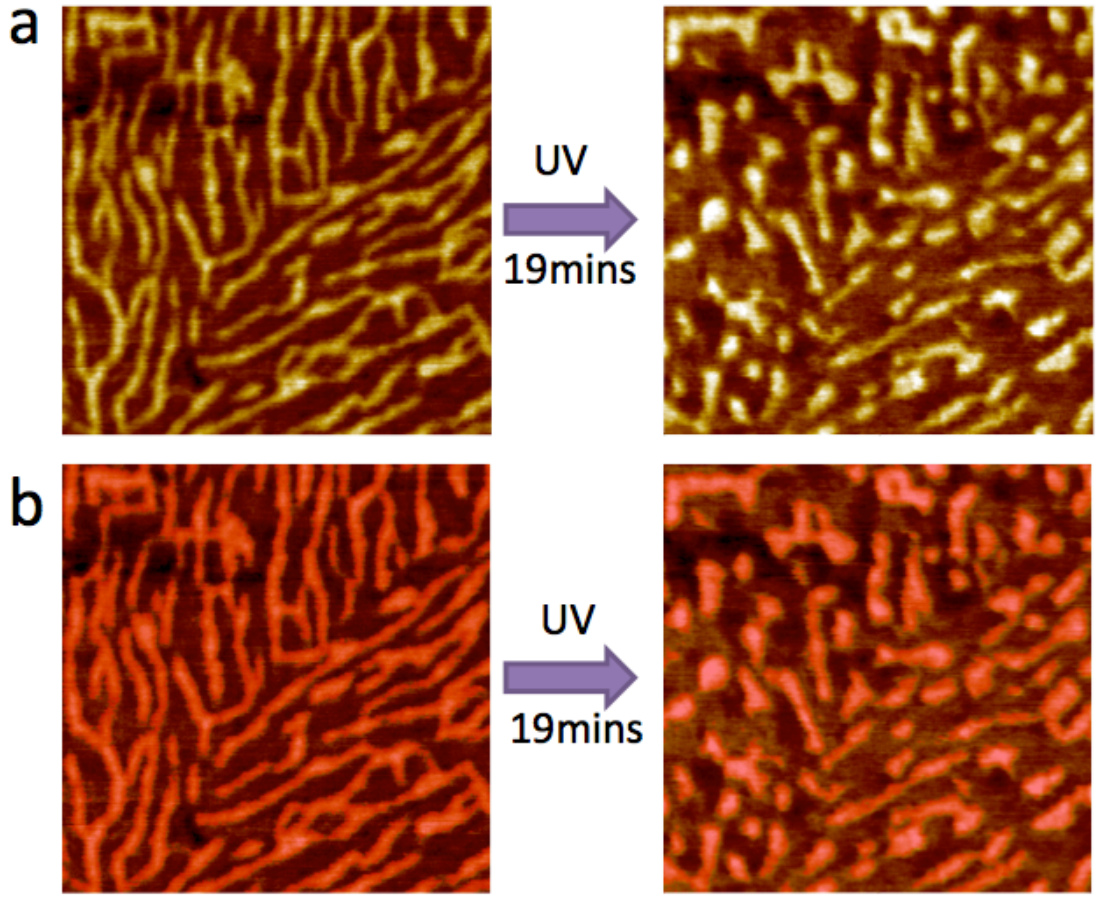

Figure A3 (a) SFM images of **P1** polymers on ODA of the same area (475nm×475nm) before and after UV irradiation. (b) **P1** areas before and after UV irradiation are marked by red color upon setting a height threshold of 0.3 nm. The surface area of **P1** polymers decreased by 23.2%.

In Figure A3, two SFM images of **P1** polymers on ODA of the same area (475nm×475nm) are extracted from **Movie S1** at 0 min and 19 min, respectively. The polymer areas are selected by setting height threshold of 0.3 nm. The **P1** areas before and after UV irradiation are 93.1 mm^2 and 71.5 mm^2, resulting in average area shrinkage of 23.2%.

Appendix III: Influence of temperature on P1 polymers and ODA

Temperature is also a factor that may affect the dynamics of polymers on a surface. Incident light on a sample may raise the local temperature of the sample up to few degrees of Celsius, depending on the intensity of irradiating light. Therefore, it is necessary to check if a changing temperature may cause the observed molecular movements.

The graphite substrate was glued onto a metal pad that could be heated up *ex-situ* by a thermal heating controller. Once the desired higher temperature was reached, the sample was kept in this temperature for 10 minutes to allow the entire sample to reach thermal equilibrium, and then it was cooled down to room temperature before performing SFM imaging. It is important to let the sample cool down to room temperature to avoid thermal drift during SFM imaging. The results are presented in Figure A4.

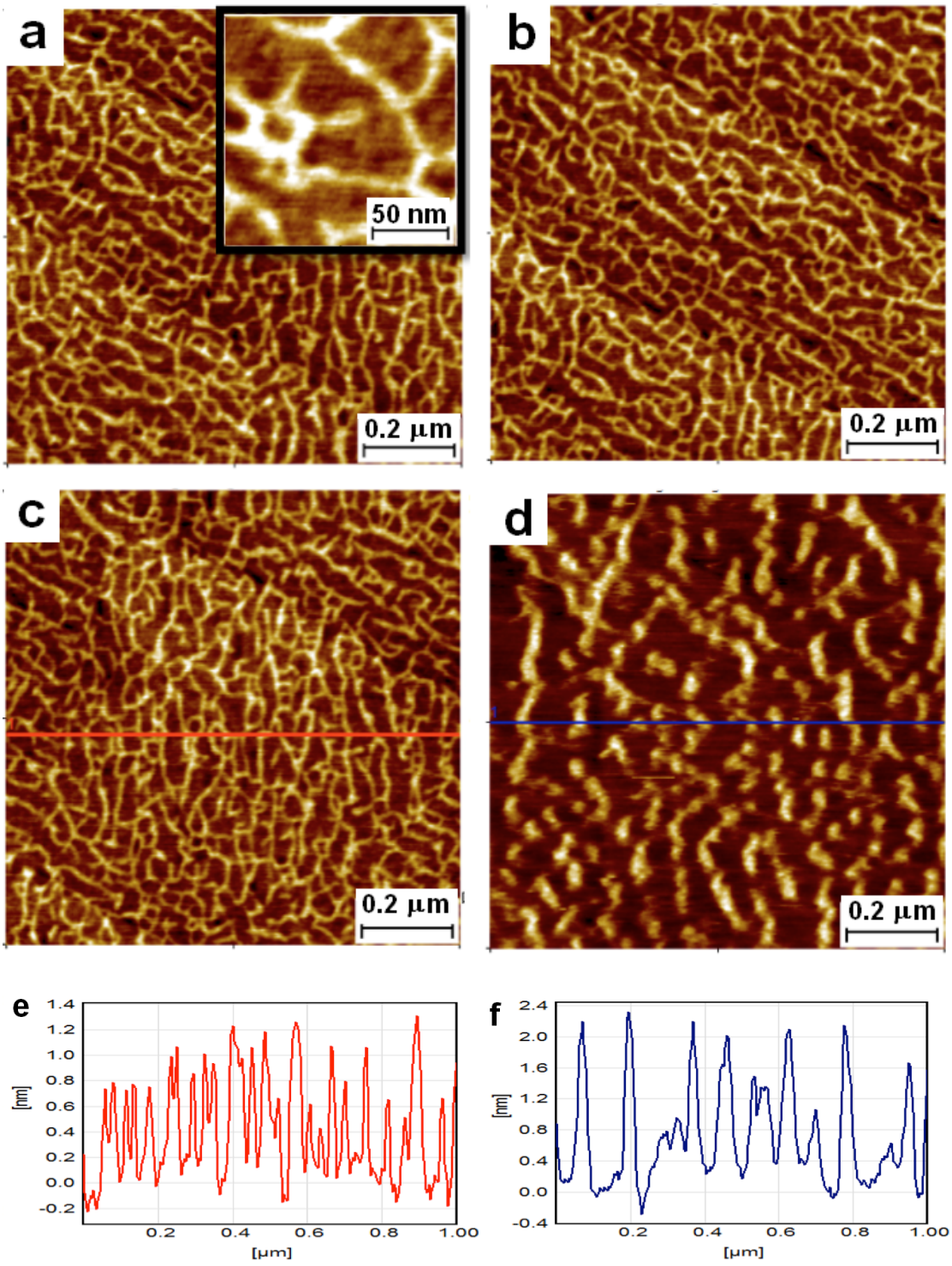

Figure A4 SFM images (1µm × 1µm) of **P1** polymers on an ODA monolayer measured at room temperature (22°C) with pretreatment of (a) without heating, (b) heating up to 35°C, (c) heating up to 45°C, and (d) heating up to 55°C, respectively. (e) Cross section along the red line in (c) showing that **P1** polymers exhibit a height around 1 nm. (f) Cross section along the blue line in (d) showing that **P1** aggregates exhibit a height around 2 nm.

Figure A4 (a) shows that at initial room temperature of 22°C, **P1** polymers lie straight on ODA lamella (inset in (a) shows lamellar structure). Then the sample is heated up *ex-situ* to 35°C and 45°C, consecutively, and cooled down for SFM imaging (Figure A4 (b) and (c)). It is clearly seen that both the morphology and the heights of **P1** polymers (around 1 nm see Figure A4 (e)) do not change noticeably even at a temperature as high as 45°C. This result suggests that the sample should not be sensitive to temperature variations that may occur during light irradiation.

Giving the fact that ODA has a melting point of 52°C, I pushed the sample beyond its limit by heating it up to 55°C. I expect that the ODA monolayer was melted at this temperature and **P1** polymers could float around on the melted ODA surface. After cooling down, the SFM image was taken (Figure A4 (d)) and it showed that the morphology of the **P1** polymers had changed from rod-like to fatter and rounder objects. The 1μm long height cross-section along blue line in (d) shows less dense objects on the surface. The heights of theses objects are around 2 nm, which is twice as high as that in Figure A4 (e). It is most likely that the **P1** polymers underwent a process of aggregation, in which the neighboring polymers have agglomerated together and formed such aggregates.

Unlike to the irradiation at different wavelengths, where the lamellar structure is always present, I do not find an ODA lamellar structure in (d) even in a zoom-in image, which suggests that the ODA molecules have melted and that rearrangement was still taking place when the image was taken.

Links for Movie S1 and Movie S2

Movie S1

http://pubs.acs.org/doi/suppl/10.1021/nn505325w

Movie S2

https://cloud.physik.hu-berlin.de/index.php/s/i0UIuaVftPWuIO4

Bibliography

(1) V. Balzani, A. C. and M. V. *Molecular Devices and Machines—Concepts and Perspectives for the Nanoworld*; Wiley-VCH, Weinheim, 2008.

(2) Davis, A. P. Synthetic Molecular Motorse. *Nature* **1999**, *401*, 120–121.

(3) Browne, W. R.; Feringa, B. L. Making Molecular Machines Work. *Nat. Nanotechnol.* **2006**, *1*, 25–35.

(4) Kay, E. R.; Leigh, D. a; Zerbetto, F. Synthetic Molecular Motors and Mechanical Machines. *Angew. Chem. Int. Ed. Engl.* **2007**, *46*, 72–191.

(5) Chiaravalloti, F.; Gross, L.; Rieder, K.-H.; Stojkovic, S. M.; Gourdon, A.; Joachim, C.; Moresco, F. A Rack-and-Pinion Device at the Molecular Scale. *Nat. Mater.* **2007**, *6*, 30–33.

(6) Brouwer, a M.; Frochot, C.; Gatti, F. G.; Leigh, D. a; Mottier, L.; Paolucci, F.; Roffia, S.; Wurpel, G. W. Photoinduction of Fast, Reversible Translational Motion in a Hydrogen-Bonded Molecular Shuttle. *Science (80-.).* **2001**, *291*, 2124–2128.

(7) Collin, J.; Dietrich-buchecker, C.; Jimenez-molero, M. C.; Sauvage, J. Shuttles and Muscles : Linear Molecular Machines Based on Transition Metals † Its Axle under the Action of an. **2001**, 477–487.

(8) Huang, T. J.; Brough, B.; Ho, C.-M.; Liu, Y.; Flood, A. H.; Bonvallet, P. a; Tseng, H.-R.; Stoddart, J. F.; Baller, M.; Magonov, S. A Nanomechanical Device Based on Linear Molecular Motors. *Appl. Phys. Lett.* **2004**, *85*, 5391.

(9) S. Shinkai, T. Nakaji, T. Ogawa, K. S. and O. M. Photoresponsive Crown Ethers. 2. Photocontrol of Ion Extraction and Ion Transport by a Bis(crown Ether) with a Butterfly-like Motion. *J. Am. Chem. Soc* **1981**, *103*, 111–115.

(10) Muraoka, T.; Kinbara, K.; Aida, T. Mechanical Twisting of a Guest by a Photoresponsive Host. *Nature* **2006**, *440*, 512–515.

(11) Nanocars, S.; Shirai, Y.; Osgood, A. J.; Zhao, Y.; Kelly, K. F.; Tour, J. M. Directional Control in Thermally Driven Single-Molecule Nanocars. *Nano Lett.* **2005**, *5*, 1–5.

(12) Kudernac, T.; Ruangsupapichat, N.; Parschau, M.; Maciá, B.; Katsonis, N.; Harutyunyan, S. R.; Ernst, K.-H.; Feringa, B. L. Electrically Driven Directional Motion of a Four-Wheeled Molecule on a Metal Surface. *Nature* **2011**, *479*, 208–211.

(13) Joachim, C. R. G. Molecule Concept Nanocars : Chassis , Wheels, and Motors? **2013**, *7*, 11–14.

(14) Weiss, P. S. Nano Races, Prizes, and Awards. *ACS Nano* **2014**, *8*, 1–1.

(15) Liu, Y.; Flood, A. H.; Bonvallet, P. a; Vignon, S. a; Northrop, B. H.; Tseng, H.-R.; Jeppesen, J. O.; Huang, T. J.; Brough, B.; Baller, M.; et al. Linear Artificial Molecular Muscles. *J. Am. Chem. Soc.* **2005**, *127*, 9745–9759.

(16) Du, G.; Moulin, E.; Jouault, N.; Buhler, E.; Giuseppone, N. Muscle-like Supramolecular Polymers: Integrated Motion from Thousands of Molecular Machines. *Angew. Chem. Int. Ed. Engl.* **2012**, *51*, 12504–12508.

(17) Hugel, T.; Holland, N. B.; Cattani, A.; Moroder, L.; Seitz, M.; Gaub, H. E. Single-Molecule Optomechanical Cycle. *Science (80-.).* **2002**, *296*, 1103–1106.

(18) Tsuchiya, S. Intramolecular Electron Transfer of Diporphyrins Comprised of Electron-Deficient Porphyrin and Electron-Rich Porphyrin with Photocontrolled Isomerization. *J. Am. Chem. Soc.* **1999**, *121*, 48–53.

(19) Steinem, C.; Janshoff, A.; Vollmer, M. S.; Ghadiri, M. R. Reversible

Photoisomerization of Self-Organized Cylindrical Peptide Assemblies at Air–Water and Solid Interfaces. *Langmuir* **1999**, *15*, 3956–3964.

(20) Ferri, V.; Elbing, M.; Pace, G.; Dickey, M. D.; Zharnikov, M.; Samorì, P.; Mayor, M.; Rampi, M. A. Light-Powered Electrical Switch Based on Cargo-Lifting Azobenzene Monolayers. *Angew. Chemie* **2008**, *120*, 3455–3457.

(21) Denise M. Junge and Dominic V. McGrath. Photoresponsive Dendrimers. *Chem. Commun.* **1997**, 857–858.

(22) D.M. Junge and D. V. McGrath. Photoresponsive Azobenzene-Containing Dendrimers with Multiple Discrete States. *J. Am. Chem. Soc.* **1999**, *121*, 4912–4913.

(23) Sheng Li and Dominic V. McGrath. Effect of Macromolecular Isomerism on the Photomodulation of Dendrimer Properties. *J. Am. Chem. Soc.* **2000**, *122*, 6795–6796.

(24) L. X. Liao, F. S. and D. V. M. Photoswitchable Flexible and Shape-Persistent Dendrimers: Comparison of the Interplay between a Photochromic Azobenzene Core and Dendrimer Structure. *J. Am. Chem. Soc* **2004**, *126*, 2181–2185.

(25) Bléger, D.; Liebig, T.; Thiermann, R.; Maskos, M.; Rabe, J. P.; Hecht, S. Light-Orchestrated Macromolecular “accordions”: Reversible Photoinduced Shrinking of Rigid-Rod Polymers. *Angew. Chem. Int. Ed. Engl.* **2011**, *50*, 12559–12563.

(26) Lee, C. L.; Liebig, T.; Hecht, S.; Bléger, D.; Rabe, J. P. Light-Induced Contraction and Extension of Single Macromolecules on a Modified Graphite Surface. *ACS Nano* **2014**, *8*, 11987–11993.

(27) Schill., G. *Catenanes, Rotaxanes and Knots*; Academic Press, New York, 1971.

(28) Schill, G.; Zollenkopf, H. Rotaxan-Verbindungen, I. *Justus Liebigs Ann. Chem.* **1969**, *721*, 53–74.

(29) Muraoka, T.; Kinbara, K.; Kobayashi, Y.; Aida, T. Light-Driven Open–Close Motion of Chiral Molecular Scissors. *J. Am. Chem. Soc.* **2003**, *125*, 5612–5613.

(30) Yu, Y.; Nakano, M.; Ikeda, T. Directed Bending of a Polymer Film by Light. *Nature* **2003**, *425*, 2003.

(31) Iamsaard, S.; Aßhoff, S. J.; Matt, B.; Kudernac, T.; Cornelissen, J.; Fletcher, S. P.; Katsonis, N. Conversion of Light into Macroscopic Helical Motion. *Nat. Chem.* **2014**, *6*, 229–235.

(32) Yamada, M.; Kondo, M.; Mamiya, J.; Yu, Y.; Kinoshita, M.; Barrett, C. J.; Ikeda, T. Photomobile Polymer Materials: Towards Light-Driven Plastic Motors. *Angew. Chem. Int. Ed. Engl.* **2008**, *47*, 4986–4988.

(33) Kobatake, S.; Takami, S.; Muto, H.; Ishikawa, T.; Irie, M. Rapid and Reversible Shape Changes of Molecular Crystals on Photoirradiation. *Nature* **2007**, *446*, 778–781.

(34) Koshima, H.; Ojima, N.; Uchimoto, H. Mechanical Motion of Azobenzene Crystals uponPhotoirradiation. *J. Am. Chem. Soc.* **2009**, *131*, 6890–6891.

(35) Bushuyev, O. S.; Tomberg, A.; Friščić, T.; Barrett, C. J. Shaping Crystals with Light: Crystal-to-Crystal Isomerization and Photomechanical Effect in Fluorinated Azobenzenes. *J. Am. Chem. Soc.* **2013**, *135*, 12556–12559.

(36) Guerrero, L.; Smart, O. S.; Woolley, G. A.; Allemann, R. K. Photocontrol of DNA Binding Specificity of a Miniature Engrailed Homeodomain. *J. Am. Chem. Soc.* **2005**, *127*, 15624–15629.

(37) Hoersch, D.; Roh, S.-H.; Chiu, W.; Kortemme, T. Reprogramming an ATP-

Driven Protein Machine into a Light-Gated Nanocage. *Nat. Nanotechnol.* **2013**, *8*, 928–932.

(38) Han, M.; Ishikawa, D.; Honda, T. Direct Visualization of Molecular Conformation Changes. *Soft Matter* **2011**, *7*, 10594.

(39) Kumar, A. S.; Ye, T.; Takami, T.; Yu, B.-C.; Flatt, A. K.; Tour, J. M.; Weiss, P. S. Reversible Photo-Switching of Single Azobenzene Molecules in Controlled Nanoscale Environments. *Nano Lett.* **2008**, *8*, 1644–1648.

(40) Zheng, Y. B.; Pathem, B. K.; Hohman, J. N.; Thomas, J. C.; Kim, M.; Weiss, P. S. Photoresponsive Molecules in Well-Defined Nanoscale Environments. *Adv. Mater.* **2013**, *25*, 302–312.

(41) Alemani, M.; Peters, M. V; Hecht, S.; Rieder, K.-H.; Moresco, F.; Grill, L. Electric Field-Induced Isomerization of Azobenzene by STM. *J. Am. Chem. Soc.* **2006**, *128*, 14446–14447.

(42) Bléger, D.; Ciesielski, A.; Samorì, P.; Hecht, S. Photoswitching Vertically Oriented Azobenzene Self-Assembled Monolayers at the Solid-Liquid Interface. *Chemistry* **2010**, *16*, 14256–14260.

(43) Dri, C.; Peters, M. V; Schwarz, J.; Hecht, S.; Grill, L. Spatial Periodicity in Molecular Switching. *Nat. Nanotechnol.* **2008**, *3*, 649–653.

(44) Comstock, M. J.; Levy, N.; Kirakosian, A.; Cho, J.; Lauterwasser, F.; Harvey, J. H.; Strubbe, D. a; Frechet, J. M. J.; Trauner, D.; Louie, S. G.; et al. Reversible Photomechanical Switching of Individual Engineered Molecules at a Surface. *Phys. Rev. Lett.* **2006**, *99*, 1–4.

(45) Choi, B.-Y.; Kahng, S.-J.; Kim, S.; Kim, H.; Kim, H. W.; Song, Y. J.; Ihm, J.; Kuk, Y. Conformational Molecular Switch of the Azobenzene Molecule: A Scanning Tunneling Microscopy Study. *Phys. Rev. Lett.* **2006**, *96*, 156106.

(46) Alemani, M.; Selvanathan, S.; Ample, F.; Peters, M. V; Rieder, K.; Moresco, F.; Joachim, C.; Hecht, S.; Grill, L. Adsorption and Switching Properties of Azobenzene Derivatives on Different Noble Metal Surfaces : Au (111), Cu (111), and Au (100). **2008**, 10509–10514.

(47) Venancio-marques, A.; Bergen, A.; Rossi-gendron, C.; Rudiuk, S.; Baigl, D. Photosensitive Polyamines for High- Performance Photocontrol of DNA. *ACS Nano* **2014**, *8*, 3654–3663.

(48) Bléger, D.; Yu, Z.; Hecht, S. Toward Optomechanics: Maximizing the Photodeformation of Individual Molecules. *Chem. Commun. (Camb).* **2011**, *47*, 12260–12266.

(49) Rau, H. Photochemistry and Photophysics. In *Photoisomerization of Azobenzenes*; Rebek, J., Ed.; Boca Raton (FL): CRC Press, 1990; pp. 119–141.

(50) Mita, I.; Horie, K.; Hirao, K. Photochemistry in Polymer Solids. 9. Photoisomerization of Azobenzene in a Polycarbonate Film. *Macromolecules* **1898**, *22*, 558–563.

(51) Schulze, F.; Petrick, H.; Cammenga, H.; Klinge, H. Thermodynamic Properties of the Structural Analogues Benzo [c] Cinnoline, Trans-Azobenzene, and Cis-Azobenzene. *Zeitschrift für Phys. Chemie* **1977**, *107*, 1–19.

(52) Monti, S.; Orlandi, G.; Palmieri, P. Features of the Photochemically Active State Surfaces of Azobenzene. *Chem Phys* **1982**, *71*, 87–99.

(53) Rau, H. Further Evidence for Rotation in the Π,π* and Inversion in the N,π* Photoisomerization of Azobenzenes. *J. Photochem.* **1984**, *26*, 221–225.

(54) Nägele, T.; Hoche, R.; Zinth, W.; Wachtveitl, J. Femtosecond Photoisomerization of Cis-Azobenzene. *Chem. Phys. Lett.* **1997**, *272*, 489–

495.

(55) Fujino, T.; Tahara, T. Picosecond Time-Resolved Raman Study of Trans-Azobenzene. *J. Phys. Chem. A* **2000**, *104*, 4203–4210.

(56) Fujino, T.; Arzhantsev, S.; Tahara, T. Femtosecond Time-Resolved Fluorescence Study of Photoisomerization of Trans-Azobenzene. *J. Phys. Chem. A* **2001**, *105*, 8123–8129.

(57) Ho, C.-H.; Yang, K.-N.; Lee, S.-N. Mechanistic Study of Trans⇆cis Isomerization of the Substituted Azobenzene Moiety Bound on a Liquid-Crystalline Polymer. *J. Polym Sci, Part A* **2001**, *39*, 2296–2307.

(58) Angeli, C.; Cimiraglia, R.; Hofmann, H.-J. On the Competition between the Inversion and Rotation Mechanisms in the Cis-Trans Thermal Isomerization of Diazene. *Chem. Phys. Lett.* **1996**, *259*, 276–282.

(59) Jursic, B. Ab Initio and Density Functional Theory Study of the Diazene Isomerization. *Chem. Phys. Lett.* **1996**, *261*, 13–17.

(60) Naito, T.; Horie, K.; Mita, I. Photochemistry in Polymer Solids. 11. The Effects of the Size of Reaction Groups and the Mode of Photoisomerization on Photochromic Reactions in Polycarbonate Film. *Macromolecules* **1991**, *24*, 2907–2911.

(61) Lamarre, L.; Sung, C. S. P. Studies of Physical Aging and Molecular Motion by Azochromophoric Labels Attached to the Main Chains of Amorphous Polymers. *Macromolecules* **1983**, *16*, 1729–1736.

(62) Weiss, R. G.; Ramamurthy, V.; Hammond, G. S. Photochemistry in Organized and Confining Media: A Model. *Acc. Chem. Res.* **1993**, *26*, 530–536.

(63) Zhao, Y.; Tomiki, I. *Smart Light-Responsive Materials: Azobenzene-*

Containing Polymers and Liquid Crystals; 1st ed.; John Wiley & Sons, Inc., 2009.

(64) Deloncle, R.; Caminade, A. M. Stimuli-Responsive Dendritic Structures: The Case of Light-Driven Azobenzene-Containing Dendrimers and Dendrons. *J. Photochem. Photobiol. C Photochem. Rev.* **2010**, *11*, 25–45.

(65) Liao, L.-X.; Stellacci, F.; McGrath, D. V. Photoswitchable Flexible and Shape-Persistent Dendrimers: Comparison of the Interplay between a Photochromic Azobenzene Core and Dendrimer Structure. *J. Am. Chem. Soc.* **2004**, *126*, 2181–2185.

(66) Grebel-Koehler, D.; Liu, D.; Feyter, S. De; Enkelmann, V.; Weil, T.; Engels, C.; Samyn, C.; Müllen, K.; Schryver, F. C. De. Synthesis and Photomodulation of Rigid Polyphenylene Dendrimers with an Azobenzene Core. *Macromolecules* **2003**, *36*, 578–590.

(67) Bléger, D.; Dokić, J.; Peters, M. V; Grubert, L.; Saalfrank, P.; Hecht, S. Electronic Decoupling Approach to Quantitative Photoswitching in Linear Multiazobenzene Architectures. *J. Phys. Chem. B* **2011**, *115*, 9930–9940.

(68) Mcgonigal, G. C.; Bernhardt, R. H.; Thomson, D. J. Imaging Alkane Layers at the Liquid / Graphite Interface with the Scanning tunneUng Microscope.

(69) Rabe, J. P.; Buchholz, S. Commensurability and Mobility in Two-Dimensional Molecular Patterns on Graphite. *Science (80-.).* **1991**, *253*, 424–427.

(70) A., W.; H.-J., C.; S. N., M. Scanning Tunneling Microscopy of Alkane Adsorbates at the Liquid/graphite Interface. *Langmuir* **1993**, *9*, 2778–2781.

(71) Venkataraman, B.; Flynn, G. W.; Wilbur, J. L.; Folkers, J. P.; Whitesides, G. M.

Differentiating Functional Groups with the Scanning Tunneling Microscope. *J. Phys. Chem.* **1995**, *99*, 8684–8689.

(72) Rabe, J. P. Molecular Workbench for Imaging and Manipulation of Single Macromolecules and Their Complexes with the Scanning Force Microscope. *Top. Curr. Chem.* **2008**, *285*, 77–102.

(73) Cyr, D. M.; Venkataraman, B.; Flynn, G. W.; Black, A.; Whitesides, G. M. Functional Group Identification in Scanning Tunneling Microscopy of Molecular Adsorbates. *J. Phys. Chem.* **1996**, *100*, 13747–13759.

(74) Severin, N.; Okhapkin, I. M.; Khokhlov, A. R.; Rabe, J. P. Adsorption of Polyelectrolyte Molecules to a Nanostructured Monolayer of Amphiphiles. *Nano Lett.* **2006**, *6*, 1018–1022.

(75) Severin, N.; Barner, J.; Kalachev, A. A.; Rabe, J. P. Manipulation and Overstretching of Genes on Solid Substrates. *Nano Lett.* **2004**, *4*, 577–579.

(76) Dubrovin, E. V; Gerritsen, J. W.; Zivkovic, J.; Yaminsky, I. V; Speller, S. The Effect of Underlying Octadecylamine Monolayer on the DNA Conformation on the Graphite Surface. *Colloids Surf. B. Biointerfaces* **2010**, *76*, 63–69.

(77) *As Measured by GPC in THF vs Polystyrene (PS) Standards; Nevertheless, Owing to the Rigid-Rod Character of PPPs, Their Molecular Weight Is Most Likely Overestimated by a Factor of 1.5?2 Using GPC Calibrated with Flexible PS Standards. See Ref 39.*

(78) Butt, H.-J., Guckenberger, R., Rabe, J. p. Quantitative Scanning Tunneling Microscopy and Scanning Force Microscopy of Organic Materials. *Ultramicroscopy* **1992**, *46*, 375–393.

(79) Severin, N.; Barner, J.; Kalachev, A. A.; Rabe, J. P. Manipulation and Overstretching of Genes on Solid Substrates. *Nano Lett.* **2004**, *4*, 577–579.

(80) Weber, C.; Liebig, T.; Gensler, M.; Pithan, L.; Bommel, S.; Bléger, D.; Rabe, J. P.; Hecht, S.; Kowarik, S. Light-Controlled "Molecular Zippers" Based on Azobenzene Main Chain Polymers. *Macromolecules* **2015**, *1*, 150226133248009.

(81) Liu, Z.; Zhao, L.; Zu, Y.; Tan, S.; Wang, Y. M Icroscopy M Icroanalysis Unusual DNA Structures Formed on Bare Highly Oriented Pyrolytic Graphite Surfaces Studied by Atomic Force Microscopy. **2013**, 544–552.

(82) Sheiko, S. S.; Sun, F. C.; Randall, A.; Shirvanyants, D.; Rubinstein, M.; Lee, H.; Matyjaszewski, K. Adsorption-Induced Scission of Carbon-Carbon Bonds. *Nature* **2006**, *440*, 191–194.

(83) Coskun, A.; Banaszak, M.; Astumian, R. D.; Stoddart, J. F.; Grzybowski, B. a. Great Expectations: Can Artificial Molecular Machines Deliver on Their Promise? *Chem. Soc. Rev.* **2012**, *41*, 19–30.

(84) Lund, K.; Manzo, A. J.; Dabby, N.; Michelotti, N.; Johnson-Buck, A.; Nangreave, J.; Taylor, S.; Pei, R.; Stojanovic, M. N.; Walter, N. G.; et al. Molecular Robots Guided by Prescriptive Landscapes. *Nature* **2010**, *465*, 206–210.

(85) Gu, H.; Chao, J.; Xiao, S.-J.; Seeman, N. C. A Proximity-Based Programmable DNA Nanoscale Assembly Line. *Nature* **2010**, *465*, 202–205.

(86) von Delius, M.; Geertsema, E. M.; Leigh, D. a. A Synthetic Small Molecule That Can Walk down a Track. *Nat. Chem.* **2010**, *2*, 96–101.

(87) von Delius, M.; Leigh, D. a. Walking Molecules. *Chem. Soc. Rev.* **2011**, *40*, 3656–3676.

(88) Grill, L.; Rieder, K.-H.; Moresco, F.; Rapenne, G.; Stojkovic, S.; Bouju, X.; Joachim, C. Rolling a Single Molecular Wheel at the Atomic Scale. *Nat.*

Nanotechnol. **2007**, *2*, 95–98.

(89) Kudernac, T.; Ruangsupapichat, N.; Parschau, M.; Maciá, B.; Katsonis, N.; Harutyunyan, S. R.; Ernst, K.-H.; Feringa, B. L. Electrically Driven Directional Motion of a Four-Wheeled Molecule on a Metal Surface. *Nature* **2011**, *479*, 208–211.

(90) Nickel, A.; Ohmann, R.; Meyer, J.; Grisolia, M.; Joachim, C.; Moresco, F.; Cuniberti, G. Moving Nanostructures: Pulse-Induced Positioning of Supramolecular Assemblies. *ACS Nano* **2013**, *7*, 191–197.

(91) Perera, U. G. E.; Ample, F.; Kersell, H.; Zhang, Y.; Vives, G.; Echeverria, J.; Grisolia, M.; Rapenne, G.; Joachim, C.; Hla, S.-W. Controlled Clockwise and Anticlockwise Rotational Switching of a Molecular Motor. *Nat. Nanotechnol.* **2013**, *8*, 46–51.

(92) Chiang, P.-T.; Mielke, J.; Godoy, J.; Guerrero, J. M.; Alemany, L. B.; Villagómez, C. J.; Saywell, A.; Grill, L.; Tour, J. M. Toward a Light-Driven Motorized Nanocar: Synthesis and Initial Imaging of Single Molecules. *ACS Nano* **2012**, *6*, 592–597.

(93) Bandara, H. M. D.; Burdette, S. C. Photoisomerization in Different Classes of Azobenzene. *Chem. Soc. Rev.* **2012**, *41*, 1809–1825.

(94) Klajn, R. Immobilized Azobenzenes for the Construction of Photoresponsive Materials. *Pure Appl. Chem.* **2010**, *82*, 2247–2279.

(95) Kumaki, J.; Hashimoto, T. Conformational Change in an Isolated Single Synthetic Polymer Chain on a Mica Surface Observed by Atomic Force Microscopy. *J. Am. Chem. Soc.* **2003**, *125*, 4907–4917.

(96) Gallyamov, M. O.; Tartsch, B.; Khokhlov, a R.; Sheiko, S. S.; Borner, H. G.; Matyjaszewski, K.; Möller, M. Conformational Dynamics of Single

Molecules Visualized in Real Time by Scanning Force Microscopy: Macromolecular Mobility on a Substrate Surface in Different Vapours. *J. Microsc.* **2004**, *215*, 245–256.

(97) Kumaki, J.; Kawauchi, T.; Yashima, E. Peculiar "Reptational" Movements of Single Synthetic Polymer Chains on Substrate Observed by SFM. *Macromol. Rapid Commun.* **2008**, *29*, 406–411.

(98) Zhou, X.-L.; Zhu, X.-Y.; White, J. M. Photochemistry at Adsorbate/metal Interfaces. *Surf. Sci. Rep.* **1991**, *13*, 73–220.

(99) Adamcik, J.; Tobenas, S.; Santo, G. Di; Klinov, D.; Dietler, G. Temperature-Controlled Assembly of High Ordered / Disordered Dodecylamine Layers on HOPG : Consequences for DNA Patterning. *Langmuir* **2009**, 3159–3162.

(100) Carter, N. J.; Cross, R. A. Kinesin's Moonwalk. *Curr Opin Cell Biol.* **2006**, *18*, 61–67.

(101) Toprak, E.; Yildiz, A.; Tonks, M.; Rosenfeld, S. S.; Selvin, P. R. Why Kinesin Is so Processive. **2009**, *106*, 12717–12722.

Acknowledgement

I would like to thank *Prof. Dr. Jürgen P. Rabe* for providing me this great opportunity to enter the macromolecular world. His careful supervision, continued support and tireless revising of my thesis have all made this work possible.

I would like to acknowledge the contribution of following people in this work:

Dr. David Bléger for fruitful discussions, criticisms and comments. He does not only provide me the azobenzene-polymers, but also allow me to include some of his results in the section of "Characterization of **P1** polymers in solution". I also like to thank *Prof. Stefan Hecht* for his encouragement and allowing this cooperation between our groups.

I am thankful to *Tobias Liebig* for his initial ideal of switching macromolecules on an ODA surface. His sharing of the difficulties he encountered has helped me to setup an experimental scheme in a right direction. I also thank *Dr. Hua Liang* for sharing his tips in preparing the samples. I surely learned a lot of knowledge about macromolecules from him.

Much thank to *Dr. Nikolai Severin* and *Dr. Stefan Kirstein* for the fruitful discussions and practical help in the lab. Their experimental experiences helped me to overcome many difficulties in experiments.

I would like to thank especially my colleague *Egon Steeg*, who introduced me the interesting German culture and language. He also helped in translation German Zusammenfassung. Thanks to *Manuel Gensler*, who also helped in translation and rendered many constructive suggestions, as well as practical help in the lab.

At this point, I could not but be very grateful to my wife, *Hui-Chun Lin*, for walking this long journey with me. Without her support, encouragement and love it would have not been possible to complete this doctorate work.

Finally, much thank to *the church in Berlin*. All your prayer and loving care have supported me to go on. We truly are God's family and standing together for His testimony on earth.

Selbständigkeitserklärung

Ich erkläre, dass ich die Dissertation selbständig und nur unter Verwendung der von mir gemäß § 7 Abs. 3 der Promotionsordnung der Mathematisch-Naturwissenschaftlichen Fakultät, veröffentlicht im Amtlichen Mitteilungsblatt der Humboldt-Universität zu Berlin Nr. 126/2014 am 18.11.2014 angegebenen Hilfsmittel angefertigt habe.

Berlin, 27. Februar 2017 Chien-Li, Lee